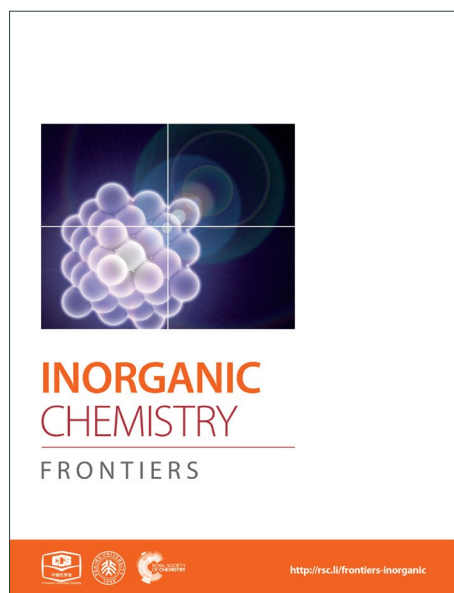
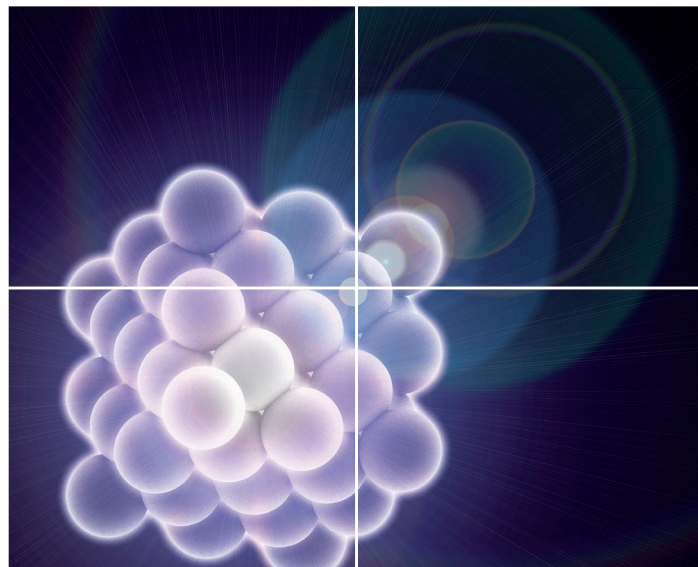


# INORGANIC CHEMISTRY

FRONTIERS

Accepted Manuscript



This is an *Accepted Manuscript*, which has been through the Royal Society of Chemistry peer review process and has been accepted for publication.

*Accepted Manuscripts* are published online shortly after acceptance, before technical editing, formatting and proof reading. Using this free service, authors can make their results available to the community, in citable form, before we publish the edited article. We will replace this *Accepted Manuscript* with the edited and formatted *Advance Article* as soon as it is available.

You can find more information about *Accepted Manuscripts* in the [Information for Authors](#).

Please note that technical editing may introduce minor changes to the text and/or graphics, which may alter content. The journal's standard [Terms & Conditions](#) and the [Ethical guidelines](#) still apply. In no event shall the Royal Society of Chemistry be held responsible for any errors or omissions in this *Accepted Manuscript* or any consequences arising from the use of any information it contains.



Journal Name

ARTICLE

## High performance electrochemical capacitor materials focusing on nickel based materials

5Received 00th January 20xx,

Bing Li,<sup>a</sup> Mingbo Zheng,<sup>a</sup> Huaiguo Xue\*<sup>a</sup> and Huan Pang\*<sup>a,b</sup>

Accepted 00th January 20xx

DOI: 10.1039/x0xx00000x

[www.rsc.org/](http://www.rsc.org/)

Of the two major capacitance contributing to the electrochemical storage devices, pseudo-capacitance which results from the reversible faradaic reactions can be much higher than the electric double layer capacitance. Transition metal compounds are emerging electrode materials for pseudo-capacitors due to their multiple oxidation states and different ions. As one of the most well-known electroactive inorganic materials, nickel based materials are being developed for this purpose. Nickel based materials have been intensively investigated and evaluated as potential electrode materials for pseudo-capacitors due to their thermal stability and chemical stability, high theoretical specific capacity, low price and environmental-friendliness. A variety of synthetic methods such as hydrothermal/solvothermal methods, sol-gel, electrodeposition, and spray deposition method have been successfully applied to prepare nickel based compounds and composite materials. In this review, comprehensively summarizes and evaluates have been given out to show the recent progress. And we introduce the nickel based compounds and composites electrode materials for supercapacitors via synthesis methods, the electrochemical performances of the electrode materials and the devices.

### 1. Introduction

Along with the social development and the improvement in human lifestyle, the demand for energy continuously increases: Energy is regarded as the most important problem facing humanity.<sup>1</sup> Successful exploitation of renewable but intermittent energy sources such as wind and solar power requires reliable and efficient electrical energy storage, so people are studying new energy storage device, with electrochemical energy storage devices being the most promising candidates.<sup>2</sup> Electrochemical energy storage technologies include batteries, fuel cells and electrochemical capacitors (ECs).<sup>3-6</sup> Based on charge storage mechanisms, ECs can be categorized into two groups: electric double layer capacitors (EDLCs) and pseudo-capacitors (also known as redox and faradaic supercapacitors).<sup>7</sup> Supercapacitors (SCs), with many excellent properties, can partly or completely replace the traditional chemical batteries especially in high power applications. Because of this, the country (especially in the developed countries) are sparing no effort to research and develop the supecapacitors. The United States, Japan, Russia and other countries are leading runners in the research and SC production, these countries also established a dedicated national management organization, such as USABC in the United States, SUN in Japan, REVA in Russia, etc...

Technical characteristics of supercapacitors include,<sup>8-12</sup> (1) Fast

charging, merely 10 s ~ 10 min is needed to reach more than 95 % of its rated capacity; (2) Long recycling life, deep charging and discharging cycle times can reach 500000; (3) High energy conversion efficiency, large current cycle efficiency is larger than 90 %; (4) High power density, equal to 5~10 times the power of a battery; (5) High security coefficient, can be used for a long time with little maintenance needed; (6) Good cryogenic properties, working well even at -30 °C; (7) Convenient detection, remaining power can be read directly. Supercapacitors are widely used in applications including,<sup>13-20</sup> (1) Small current back-up power supply; (2) Solar energy warning lights, beacon light and other solar products instead of rechargeable batteries; (3) Small charging products instead of rechargeable batteries; (4) Small power electrical drive power; (5) start power supply for the electric car; (6) Wind power generation, offshore wind turbine. The basic structure of supercapacitors consist of current collectors, electrodes, electrolyte and separator. As SCs mainly rely on the electrode active material to store energy, thus the performance of the electrode is the key factors influencing the energy density and power density. The surface morphology, pore size distribution and electrical conductivity of electrode materials are the main factors influencing the performance of electrode.

Early research on electrode material has been focused on noble metal oxides (MOs) such as RuO<sub>2</sub> and IrO<sub>2</sub>. RuO<sub>2</sub> is a conductive metal oxide, with three oxidation states accessible within 1.4 V, exhibiting an impressive reported specific capacitance up to 2000 F g<sup>-1</sup>.<sup>3,21,22</sup> RuO<sub>2</sub> is known as the most effective electrode materials, but the extremely high cost and toxicity limit their applications. Hence, cheaper transition metal oxides, such as nickel oxides, cobalt oxides, manganese oxides and iron oxides, are actively studied.

<sup>a</sup>Jiangsu Engineering Technology Research Center for Polymer-Inorganics Micro/Nano Composites (PINCs), College of Chemistry and Chemical Engineering, Yangzhou University, Yangzhou, 225002, Jiangsu, China.

<sup>b</sup>College of Chemistry and Chemical Engineering, Anyang Normal University, Anyang, 455002, P. R. China

\*E-mail: [huanpanqchem@hotmail.com](mailto:huanpanqchem@hotmail.com); [panghuan@yzu.edu.cn](mailto:panghuan@yzu.edu.cn); [chhxue@yzu.edu.cn](mailto:chhxue@yzu.edu.cn)

Among them, manganese oxide is one of the most studied, due to their low cost, environment friendly, and relatively high theoretical capacitance of  $1100 \text{ F g}^{-1}$ ~ $1300 \text{ F g}^{-1}$ .<sup>23</sup> But their low density, low conductivity, and poor cycling stability associated with unsatisfactory high rate capability remain to be improved. Cobalt-based compounds and composites have been extensively studied as pseudo-capacitors, exhibiting high specific capacitances (up to  $3000 \text{ F g}^{-1}$ ),<sup>24</sup> high areal capacitance ( $25 \text{ F cm}^{-2}$ ),<sup>25</sup> large specific surface area and long cycle life.<sup>26</sup> However, the working potential window of most of the cobalt electrode material is small, which seriously affect the application of cobalt electrode materials.

Being widely used in supercapacitors, nickel based compounds and composites have also been generally studied. Nickel based materials,<sup>27</sup> in particular, nickel oxide (NiO),<sup>28,29</sup> and nickel hydroxide ( $\text{Ni(OH)}_2$ )<sup>30</sup> have attracted extra interests due to their high theoretical capacitance values (the theoretical capacitance values of NiO and  $\text{Ni(OH)}_2$  in a potential window of 0.5 V are 2573 and  $2082 \text{ F g}^{-1}$ , respectively), thermal stability and high chemical stability, environmentally benign nature, lower cost and ready availability.

The performance of nickel based pseudo-capacitor electrode materials is determined by the redox reaction of NiO or  $\text{Ni(OH)}_2$  in alkaline electrolytes, and can be generalized as equation (1) and (2):

For NiO:



For  $\text{Ni(OH)}_2$ :



The type and preparation methods of these materials are diverse, and the doping modification methods for these materials are flexible. The pseudo-capacitance of nickel-based materials is influenced by material structure, crystallinity, conductivity, electrolyte, and material loading mass on the electrode. We could improve the supercapacitance performance via controlling the materials construction, forming composites, developing new nickel based materials. This review is dedicated to this important material family, presenting a timely effort to comprehensively and critically evaluate the development, in order to promote future breakthroughs in this field.

## 2. Nickel oxide electrodes

Thanks to recent remarkable progress in nanomaterials synthesis, nanostructured metal oxides have been extensively investigated for using as electrode materials in SCs.<sup>31</sup> Among the many MOs studied so far, Nickel oxide (NiO) is especially attractive because of its high theoretical capacitance of  $2573 \text{ F g}^{-1}$ ,<sup>32</sup> resourcefulness, environmental friendliness, good thermal and chemical stability. Due to fast redox reactions, shortened diffusion paths and high specific surface areas in the solid phase, micro/nanomaterials have found wide application in electrochemical capacitors.<sup>33-37</sup> NiO nanostructures including nanowires,<sup>29</sup> nanoflowers,<sup>38</sup> nanoparticles,<sup>39</sup> nanoporous films,<sup>40</sup> and hollow nanofibers have

**Table 1** Comparison of the capacity and other important parameters of the materials in the literature

Material	Size (nm)	Surface area(m <sup>2</sup> /g)	Capacity (F/g) (low current density)	Capacity (F/g) (high current density)	Capacity retention (%)
NiO nanoflowers <sup>27</sup>	20-30	62.7	1678.4 (0.625 A/g)	856 (6.25A/g)	99.7 % (1000cycles, 6.25A/g)
NiO nanowire <sup>29</sup>	50	–	180 (0.126A/g)	–	–
NiO nanofibers/Ni <sup>31</sup>	~60	–	737 (2 A/g)	570 (40A/g)	~100% (8000 cycles, 10 A/g)
nanonet/nanoflower NiO <sup>38</sup>	–	–	840 (0.1 mA/cm <sup>2</sup> )	697 (10 mA/cm <sup>2</sup> )	–
NiO film <sup>40</sup>	–	196.8	441 (2 A/g)	200 (20 A/g)	–
NiO nanoparticle <sup>43</sup>	8	–	549 (1 mv/s)	236 (20 mv/s)	60.6 % (1000cycles, 2A/g)
NiO/Ni <sup>44</sup>	4.4	37	905 (1 A/g)	380 (28.6 A/g)	–
NiO nanorod <sup>45</sup>	–	–	2018 (2.27 A/g)	1536 (22.7 A/g)	92 % (500cycles, 50mA/cm <sup>2</sup> )

been reported as electrode materials in SCs. But the conventional binder-needed electrode design and the poor electrical conductivity of NiO largely limit ion, electron transport, making NiO-based SCs not suitable for high-rate applications.

A comparison with previously reported NiO pseudocapacitive nanomaterials is given in Table 1. The morphology of NiO is greatly important for its electrochemical performance. The porous structure could provide a very short diffusion pathway for ions as well as large active surface area, and a large surface area is associated with more Faradic active sites. It is well accepted that pseudo-capacitance is an interfacial phenomenon tightly related to the morphology of electroactive materials. For NiO nanorod arrays, the ultra-high capacitance and cycling stability may therefore be attributed to the slim nanorod, the well-aligned array structure, and the stable chemical bonding of NiO nanorods on the Ni substrate.

### 2.1 NiO nanowires

Nanowires (NWs) are one-dimensional (1D) nanostructures, which are perfect building blocks for functional nanodevices and represent the smallest dimension for efficient electron and exciton transport.<sup>41,42</sup>

Kundu et al. prepared NiO-nanofibers/Ni through electrospinning technique followed by appropriating heat treatment, the fabrication of binder-free electrodes consisting of porous NiO nanofibers directly grown on nickel foams (NFs) current collector.<sup>31</sup> The morphology of porous NiO-Nanofibers is shown in Fig. 1 (b). They found that the electrospun NiO-Nanofibers formed a porous interconnected network and were intimately attached to the Ni foam surface, enabling fast electron collection and efficient ion transport. The as-fabricated binder-free electrodes exhibited high specific capacitance of 737, 731, 679, 626, 591 and  $570 \text{ F g}^{-1}$  at current densities of 2, 5, 10, 20, 30 and  $40 \text{ A g}^{-1}$ , respectively, showing wonderful capacitance retention at high current rates. The NiO-Nanofibers/Ni electrodes also revealed super cycling stability up to 8000 cycles without discernable capacitance fading at various current densities.

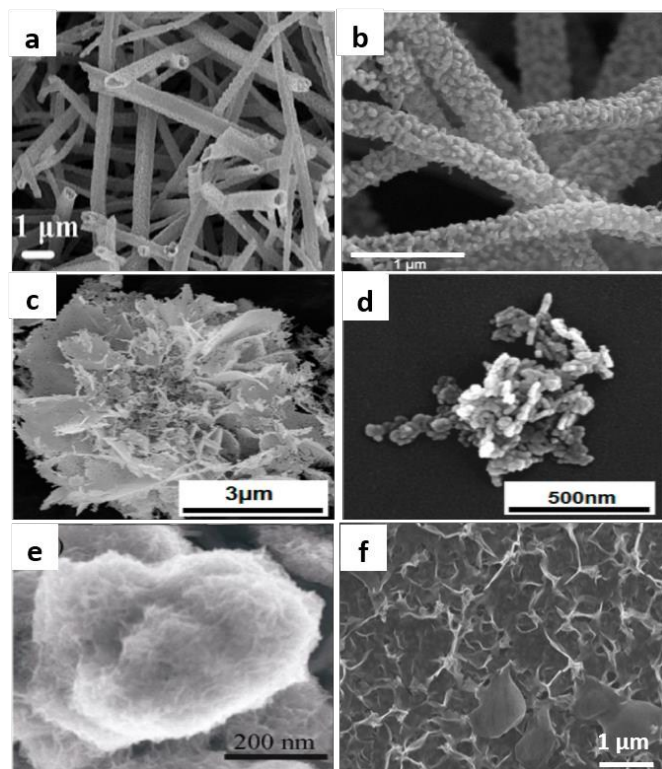


**Fig. 1** SEM image of (a) NiO nanotubes obtained by calcining the  $\text{Ni}(\text{dmg})_2$  nanorods; (b) porous NiO-Nanofibers; (c) NiO nanoflowers; (d) NiO nanoparticle; (e) NiO/Ni films after annealing at 673 K; (f) NiO thin film. (a) Adapt with the permission from ref. 28, ©2009 The Royal Society of Chemistry; (b) ref. 31, ©2015 elsevier; (c, d) ref. 37, © 2013 American Chemical Society; (e) ref. 45, © Springer; (f) ref. 51, © 2010 Elsevier.

Pang et al. successfully synthesized NiO nanowires/Ni foil electrodes by “nanoseed-catalyzing” mechanism.<sup>29</sup> By controlling the concentration of LiOH solution, different NiO nanostructures formed on the surface of Ni foil, including nanowires, nanorods, and nanoparticles. The measurements of electrochemical properties showed that the NiO nanowires/Ni foil have the highest electrical conductivity, and the long NiO nanowires/Ni foil electrode showed fine power-storage property and good electrochemical reversibility.

## 2.2 NiO nanoflowers

Cheng et al. made hybrid nanonet/nanoflowers NiO deposited on carbon fiber paper (CFP), two types of electrodes with different morphologies were grown on the CFP by hydrothermal and electrodeposition process.<sup>38</sup>

The hybrid NiO electrodes with mass loading of  $1.1 \text{ mg cm}^{-2}$  exhibited the highest areal capacitance of  $0.93 \text{ F cm}^{-2}$  ( $\sim 840 \text{ F g}^{-1}$  of the active material and  $84 \text{ F g}^{-1}$  of total weight, including CFP current collector and substrate), which was better than most similar materials reported for supercapacitors. The hybrid electrode retained excellent rate capability at a high mass loading. For example, the areal capacitance of the hybrid electrode with NiO loading is  $0.77 \text{ F cm}^{-2}$  at a current density of  $10 \text{ mA cm}^{-2}$ , which is about 83 % of that measured at  $0.1 \text{ mA cm}^{-2}$  ( $0.93 \text{ F cm}^{-2}$ ). Typically, with the increase in discharging current density, the specific capacitance dramatically decreased (less than 50 % capacitance retention). The electrode also demonstrates an excellent cycling life

and good cycling stability. The capacitance decreased to about 70 % of the initial capacitance after 10000 cycles.

Pang et al. successfully synthesized NiO microflowers by calcining a coordination microflowers without any hard templates, seed or using soft template.<sup>27</sup> The porous NiO microflowers showed a specific capacitance of  $1678.4 \text{ F g}^{-1}$  at current density of  $0.625 \text{ A g}^{-1}$ , and maintained about 99.7 % after 1000 cycles.

## 2.3 NiO nanoparticles

Jahromi et al. synthesized NiO nanoparticles with various sizes (NPs, 8, 12, and 22 nm) via a facile sol-gel method.<sup>43</sup> They used gelatine as a green polymerizing agent, followed by calcination at various temperatures (300, 400, and 500 °C), the morphology and size distribution of these nickel oxide nanoparticles are shown in Fig. 3.

The calcination temperature played an important role in controlling the particle size. Fig. 2 (a-c) show a flake-like morphology for the NiO NPs samples, with a porous open channel within the flake. With the calcination temperature increasing, the crystallite size of the nickel oxide grew, which formed rougher and larger particles, making the close packing of the nickel oxide difficult.

The calculated specific capacitance values for NiO NPs with particle sizes of 8, 12, and 22 nm were 549, 442, and  $199 \text{ F g}^{-1}$ , respectively, at a scan rate of  $1 \text{ mV s}^{-1}$ . The histograms for the size distribution of the NiO NPs are shown in Fig. 2 (d-f), the average particle sizes of the NiO NPs were 8, 12, and 22 nm when calcined at 300, 400, and 500 °C respectively. The size effect of NiO NPs on the electrochemical performance was studied, the capacitance retention values of the NiO NPs electrodes with particle sizes of 8, 12, and 22 nm after 1000 charge/discharge cycles at a current density of  $2.0 \text{ A g}^{-1}$  were 60.6 %, 72.9 %, and 81.8 %, respectively, the results are shown in Fig. 2 (h). The NiO NPs with a 22 nm size showed good reversibility comparing to the other NiO NPs because

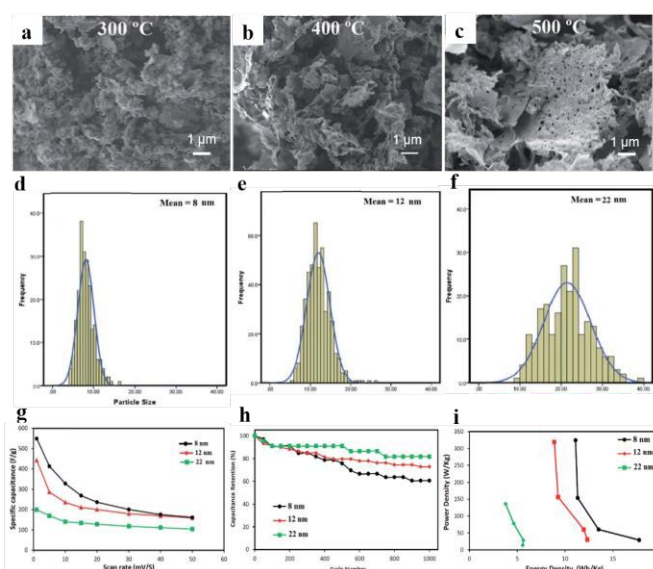


**Fig. 2** (a-c) FESEM morphological structures of NiO samples at different calcination temperatures; (d-f) the size distribution of NiO NPs calcinated at different temperature; (g) Specific capacitance of NiO NPs at different scan rate; (h) Capacitance retention for the NiO

## ARTICLE

Journal Name

NPs electrode; (i) Ragone plots of NiO NPs electrode. Adapted with permission from ref. 43, © 2015 Royal Society of Chemistry.

of the high crystalline nature when calcined at 500 °C. The Ragone plot result (Fig. 2i) demonstrated that the 8 nm NiO NPs exhibited the highest power density and energy density. The result indicated that the 8 nm NiO NPs are more suitable for supercapacitor applications compared to other samples because of the high accessibility of the OH<sup>-</sup> ions to the outer and inner pore surface at different current densities.

Lu et al. built an advanced supercapacitor electrode using a simple and scalable fabrication technique, they optimized the electrode performance using a well-defined electrode network with minimum resistivity and a controlled functional material.<sup>44</sup> Ni nanoparticles were synthesized using a modified polyol process. After a simple mechanical compaction of these as-prepared nanoparticles and a subsequent low-temperature annealing process, NiO/Ni nanoporous composite electrodes were obtained with maximized power and energy densities. The electrodes oxidized at 250 °C showed significantly better performance than their high-temperature counterparts. The average specific capacitance was calculated to be 910 F g<sup>-1</sup> from cyclic voltammetry (CV) and 905 F g<sup>-1</sup> from cyclic chronopotentiometry (CC) based on the mass of NiO, the specific capacitance drops to 348 F g<sup>-1</sup> at 300 °C and further to 72 F g<sup>-1</sup> at 350 °C. At 1 A g<sup>-1</sup> a high-energy density of 62 Wh kg<sup>-1</sup> (equivalent to 905 F g<sup>-1</sup>) was achieved. As the charge/discharge rate was increased to 28.6 A g<sup>-1</sup>, a high-power density of 10 kW kg<sup>-1</sup> was observed, although the corresponding energy density dropped to 26 Wh kg<sup>-1</sup> (equivalent to 380 F g<sup>-1</sup> for the SC).

#### 2.4 NiO nanorods

Different NiO nanostructures have been employed in supercapacitors, but designing and preparing a stable supercapacitors with high energy and power density based on this cost-effective materials remain a challenge. Lu et al. synthesized NiO nanorod arrays on Ni foam by hydrothermal method.<sup>45</sup> NiO nanorod arrays on Ni foam showed a combination of ultrahigh specific capacitance of 2018 F g<sup>-1</sup> (or 4.44 F cm<sup>-2</sup>) at a charge and discharge current density of ~2.27 A g<sup>-1</sup> (or 5 mA cm<sup>-2</sup>). This value was 80 % of theoretical value (2573 F g<sup>-1</sup>). The rate capacitance is also high, 1536 F g<sup>-1</sup> (or 3.38 F cm<sup>-2</sup>) at 22.7 A g<sup>-1</sup> (or 50 mA cm<sup>-2</sup>), indicating a high power density. Furthermore, the array-structured supercapacitors showed excellent cycling stability, only 8 % of capacitance was lost in the first 100 cycles with no further change in the subsequent 400 cycles. Combining all these virtues into one material suggested it could be used to fabricate long lifetime, cost-effective, and ultrahigh energy/power density supercapacitors.

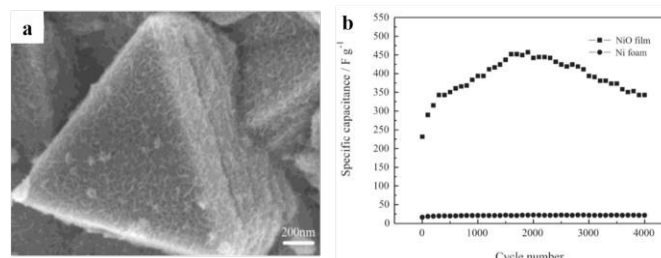


**Fig. 3** (a) SEM images of NiO films annealed at 300 °C for 2h; (b) cycling performance of NiO film and Ni foam at 2 A g<sup>-1</sup>. Adapted with permission from ref. 40, ©2012 Elsevier.

#### 2.5 Hierarchically porous NiO films

By a facile ammonia-evaporation method, Zhang et al. directly grew a hierarchically porous NiO films on nickel foam substrate. The SEM images are shown in Fig. 3.<sup>40</sup> They used 30 mL aqueous ammonia (25–28 %) added to 30 mL aqueous solution of 0.1 M Ni(NO<sub>3</sub>)<sub>2</sub>·H<sub>2</sub>O with vigorous stirring. Nickel foam substrate was pressed to thin plate by 10 MPa and cleaned ultrasonically in ethanol for 10 min. After being immersed into the reaction solution, its right side was protected by equably coating with polytetra fluoroethylene tape. After heat treatment, the nickel foam substrate was covered with a green film. Then the film was heated in tube furnace at 300 °C for 2 h in flowing argon, the specific capacitance of the porous NiO film at a galvanostatic current density of 2, 4, 10, and 20 A g<sup>-1</sup> are 232 F g<sup>-1</sup>, 229 F g<sup>-1</sup>, 213 F g<sup>-1</sup> and 200 F g<sup>-1</sup>, respectively. 87 % of capacitance is retained when the current density changes from 2 A g<sup>-1</sup> to 20 A g<sup>-1</sup>. The porous-structured NiO electrode showed an obvious increase from 232 F g<sup>-1</sup> to 349 F g<sup>-1</sup>, during the first 400 cycles, and then slightly increased to the highest specific capacitance (441 F g<sup>-1</sup>) until around 1500 cycles.

#### 2.6 NiO nanotubes

Due to high porosity, increased surface area, and low mass density, hollow inorganic nanomaterials constituted an important family of nanostructures. These hollow inorganic nanomaterials exhibit interesting properties and potential applications, such as host materials, catalysts, drug-delivery carriers, sensors, biomedical diagnosis agents, acoustic insulation and chemical reactors.<sup>46–49</sup> Pang et al. developed a convenient and simple approach for the synthesis of NiO nanotubes through 1-D metal complex bis (dimethylglyoximate) nickel (II), Ni(dmg)<sub>2</sub>.<sup>28</sup> The NiO nanotubes showed great electrochemical capacitance, magnetic properties, and anti-bacterial activities. The SEM images of NiO nanotubes are shown in Fig. 1 (a).

Kim et al. successfully synthesized porous NiO nanostructures with three distinct morphologies by a sol-gel method, the morphology of as-prepared Ni(OH)<sub>2</sub> precursor was simply directed by controlling the pH of the solution. The morphology of the porous NiO nanostructures are shown in Fig. 1 (c, d).<sup>37</sup> Electrochemical measurements showed that the nanoflower-shaped NiO which had the greatest pore volume but the lowest surface area exhibited the greatest specific pseudocapacitance. Their morphology-dependent supercapacitors properties were exploited, the NiO nanoflowers showed great specific capacitance values of 480, 381, 333, and 252 F g<sup>-1</sup>, the nanoslice exhibited values of 116, 86, 65, and 52 F g<sup>-1</sup>, and the nanoparticles gave values of 260, 235, 179, and 89 F g<sup>-1</sup> at

current densities of 0.5, 1, 2, and 5 A g<sup>-1</sup>. The excellent performance of the nanoflower-shaped NiO 3D nanonetwork can be attributed to multi-pores, which can contact with the electrolyte easily, forming nanochannels in the NiO structure, and providing longer electron pathways. This hypothesis was well-supported by the XPS and EIS data of the NiO nanostructure. The flower-shaped NiO having the lowest surface area among the three morphologies was effectively optimized as a superior electrode and yielded the greatest pseudocapacitance. This study indicated that forming a 3D nanonetwork was a straightforward mean of improving the electrochemical properties of a supercapacitors.

### 3. Nickel hydroxide materials

Among numerous active electrode materials, nickel hydroxide is recognized as promising electrode materials in electrochemical ECs.<sup>52</sup> Almost all the attention has been focused on crystalline Ni(OH)<sub>2</sub> materials mainly because of their flexibility in forming complex 3D structures and their excellent electrochemical properties in rechargeable alkaline battery applications.<sup>53</sup> Amorphous Ni(OH)<sub>2</sub> materials are usually assessed as unsuitable electrochemical capacitors because of their poor performance.<sup>54</sup> However, the amorphous phase offers a rather unique electrochemical behaviour that may be exploitable in certain device applications.<sup>55-57</sup> As shown in Table 2, the specific capacitance of Ni(OH)<sub>2</sub>-based electrode is notably high. The following is a detailed introduction of some Ni(OH)<sub>2</sub>-based materials.

**Table 2** Capacitance properties of some recent published Ni(OH)<sub>2</sub>-based electrodes materials

Material	specific capacitor (F g <sup>-1</sup> ) (Low current density/scan rate)	specific capacitor (F g <sup>-1</sup> ) (High current density/scan rate)	Capacity retention (%)
Amorphous Ni(OH) <sub>2</sub> nanosphere <sup>68</sup>	2188 (1 mV/s)	1484 (10 mV/s)	76% (10000 cycles, 100mV/s)
Ni(OH) <sub>2</sub> /Ni foam <sup>58</sup>	3152 (4 A g <sup>-1</sup> )	280 (16 A g <sup>-1</sup> )	52% (300cycles, 4 A g <sup>-1</sup> )
Nanoporous Ni(OH) <sub>2</sub> <sup>52</sup>	2200 (1 A g <sup>-1</sup> )	1299 (10 A g <sup>-1</sup> )	92.3 % (2000cycles, 1 A g <sup>-1</sup> )
Ni(OH) <sub>2</sub> /NiOOH <sup>63</sup>	1420 (2 A g <sup>-1</sup> )	1098 (40A g <sup>-1</sup> )	81 % (1000cycles, 2 A g <sup>-1</sup> )
Ni(OH) <sub>2</sub> hexagonal-Ni foam <sup>69</sup>	2534 (1 mV/s)	1082 (10 mV/s)	97% (2000cycles, 50mV/s)
Ni(OH) <sub>2</sub> -Ni nanohybrid <sup>77</sup>	1793 (1.25 A g <sup>-1</sup> )	850 (12.5 A g <sup>-1</sup> )	98.4 % (2000cycles, 5 A g <sup>-1</sup> )
Amorphous Ni(OH) <sub>2</sub> @Ni core-shell <sup>78</sup>	2868 (1 mV/s)	1980 (10 mV/s)	97% (1000cycles, 100mV/s)

#### 3.1 Micro/nanostructured Ni(OH)<sub>2</sub>

There have been numerous approaches to fabricate Ni(OH)<sub>2</sub> electrodes, among which two strategies are usually employed. One strategy is to synthesize Ni(OH)<sub>2</sub> active material, mixing it thoroughly with the binder and conducting agent to produce a paste, and then pressing the paste onto a current collector, such as nickel foam, to form the electrode.<sup>59-62</sup> This electrode fabrication process is complicated and costly. Moreover, the addition of the binder not only decreases the charge transport rate, but also increases the electrode mass. The other strategy is to deposit Ni(OH)<sub>2</sub> active material directly onto a current collector, which limits the active materials loading and often forms an inhomogeneous structure.<sup>63-66</sup> In addition, this type of electrode suffers from relatively weak adhesion between the Ni(OH)<sub>2</sub> active

materials and the current collector, leading to the loss of accessible active materials and a shorter supercapacitors electrode cycle life.<sup>64,66</sup> The above mentioned problems narrow the practical applications of the Ni(OH)<sub>2</sub> electrode materials.<sup>67</sup> Hence, developing a facile cost-effective fabrication route for the Ni(OH)<sub>2</sub> electrode material with both excellent electrode performance and high fabrication efficiency is desirable.

Li et al. synthesized amorphous Ni(OH)<sub>2</sub> nanospheres using a low-cost, simple, green technology electrochemistry technique, then fabricated various supercapacitors from these nanospheres.<sup>68</sup> Their measurements indicated that these nanospheres showed excellent electrochemical performance, including super-long cycle life, high capacitance and energy density. The measured capacitance of the amorphous Ni(OH)<sub>2</sub> nanospheres was much higher than those of α-Ni(OH)<sub>2</sub>/graphene (1735 F g<sup>-1</sup>)<sup>69</sup> and β-Ni(OH)<sub>2</sub> nanoplates/graphite (1335 F g<sup>-1</sup>).<sup>218</sup> The specific capacitances were 1868, 1626, 1544, 1430, 1404 and 1330 F g<sup>-1</sup> at current densities of 20, 30, 40, 50, 60 and 70 A g<sup>-1</sup>, respectively. Over this current density range, the specific capacitance decreased to 72 % of its initial value. At a scan rate of 100 mV s<sup>-1</sup> for 1,000 cycles the nanospheres lost only ~3 % of their initial capacitance. The capacitance was 76 % of the initial capacitance after 10000 cycles, indicating excellent long-term stability of the amorphous Ni(OH)<sub>2</sub> nanospheres electrode. These results revealed the ultrahigh specific capacitance and remarkable rate capability of the amorphous Ni(OH)<sub>2</sub> nanomaterials for high-performance electrochemical pseudo-capacitors.

Li et al. developed a facile, cost-effective green method to fabricate Ni(OH)<sub>2</sub> hexagonal platelets on Ni foam in situ as a binder-free supercapacitors electrode.<sup>70</sup> The Ni(OH)<sub>2</sub> hexagonal platelets were self-grown on 3D Ni foam by a one-step hydrothermal treatment, with the Ni foam in a 15 wt % H<sub>2</sub>O<sub>2</sub> aqueous solution without the use of nickel salts, bases, acids, or post-treatments. The as-prepared Ni(OH)<sub>2</sub> hexagonal platelets-Ni foam electrode exhibited a considerably rougher surface, as shown in Fig. 4.

The as-prepared Ni(OH)<sub>2</sub> hexagonal platelets-Ni foam electrode can be used as supercapacitor electrode materials, thereby avoiding the need for binders and conducting agents. The specific capacitances were calculated to be 2534, 1884, 1295, 1082, and 692 F g<sup>-1</sup> at scan rates of 1, 2, 5, 10 and 25 mV s<sup>-1</sup>, respectively. Such remarkable capacitances in 2.0 M KOH electrolyte might be attributed to the large surface area, large amount of loading mass and high stability of the Ni(OH)<sub>2</sub> hexagonal platelets. And 97 % capacitance remained after 2000 cycles at a scan rate of 50 mV s<sup>-1</sup>.

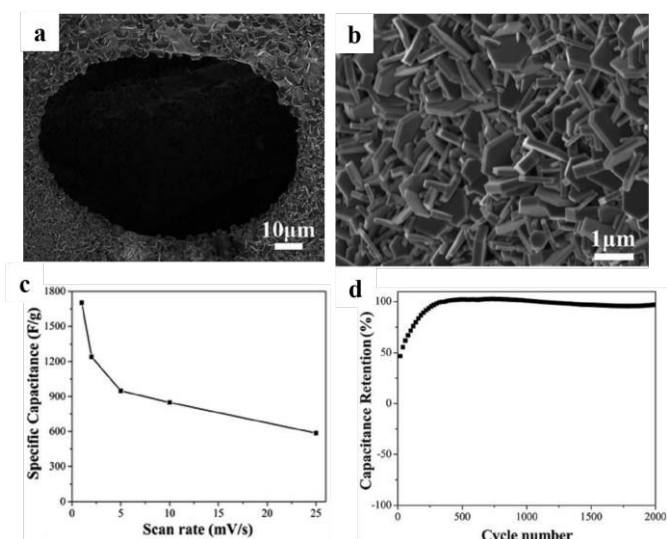


**Fig. 4** (a, b) FIB-SEM images of the Ni(OH)<sub>2</sub> hexagonal platelets-Ni foam sample surface; (c) Specific capacitance of the as-prepared Ni(OH)<sub>2</sub> material at various scan rates; (d) Cycle performance measured at a scan rate of 50 mV s<sup>-1</sup> for 2000 cycles. Adapted with permission from ref. 70, ©2015 The Royal Society of Chemistry.

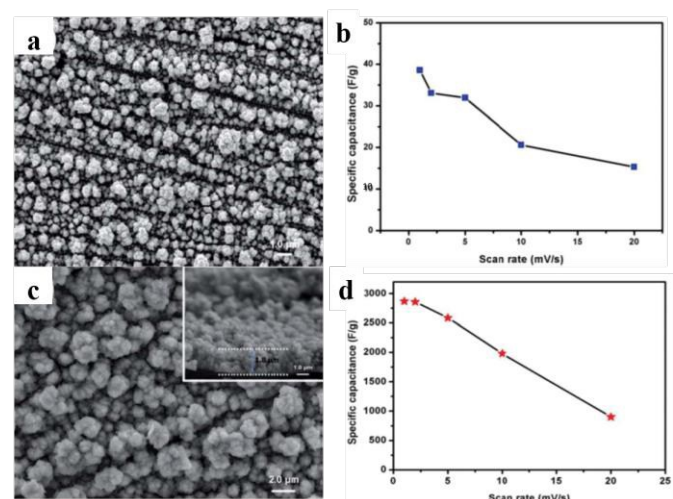


**Fig. 5** SEM images of (a) 3D nano-Ni particles; (c) Ni(OH)<sub>2</sub> @ 3D Ni core-shell composite and the inset is the crosssection image; Specific capacitance of (b) the 3D nano-Ni particles electrode, (d) Ni(OH)<sub>2</sub> @ 3D Ni core-shell electrode as function of the scan rates based on the CV curves. Adapted with permission from ref. 78, ©2015 The Royal Society of Chemistry.

### 3.2 Combining nanostructured Ni(OH)<sub>2</sub> with metal materials

In this part, we mainly introduce the Ni(OH)<sub>2</sub> nanostructure combination with micro/nanostructure metal materials, such as nanoparticles Au/Ni(OH)<sub>2</sub> and Ni(OH)<sub>2</sub>-Ni nanohybrids. The Ni(OH)<sub>2</sub>-based materials on Ni foam are excluded in this part because the size of Ni foam is too large and it is used as a current collector.

Kim et al. presented a cost-effective and easy route to overcome low conductivity and poor cycle-stability of Ni(OH)<sub>2</sub> via creation of virtual 3D conducting networks, they created the networks by simple deposition of gold nanoparticles on 3D-Ni(OH)<sub>2</sub> for pseudo-capacitor applications.<sup>71</sup> In effect, via metal/semi-conductor contacted through the interior structure of Ni(OH)<sub>2</sub>, the

partially deposited Au nanoparticles on the surface of 3D-Ni(OH)<sub>2</sub> provided a 3D conductive network. The highly conductive and bi-continuous gold networks facilitated effective transport of the electrons. The Au deposited Ni(OH)<sub>2</sub> (Au/Ni(OH)<sub>2</sub>) showed greatly increased rate capability and good cycling stability, all of which were attributed to the improved conductivity achieved by the presence of a small amount Au NPs on the surface of Ni(OH)<sub>2</sub>.

Chen et al. reported a surprising increase in specific capacitance up to 1145 F g<sup>-1</sup> and excellent cycling stability from a nanoporous Au/MnO<sub>2</sub> hybrid structure without any additive.<sup>72</sup> The outstanding enhancement in the capacitance value was mainly attributed to the presence of three dimensional conductive networks of nanoporous gold fabricated by de-alloying specific composition (Ag<sub>65</sub>Au<sub>35</sub>) of Au. Although the effects and the importance of the 3-dimensional (3D) gold nanostructures are clearly demonstrated in this report, the fabrication process was too complicated and not feasible for real applications.

Recently, Ni(OH)<sub>2</sub>/NF composites was prepared.<sup>73,71</sup> A hydrothermal method was applied to deposit ultrathin primary nanowalls of Ni(OH)<sub>2</sub> on NFs, and the composites showed a capacitance higher than the theoretical value.<sup>66</sup> Moreover, porous and 3D nanostructured Ni(OH)<sub>2</sub> were electro-deposited on NFs to synthesize the composites.<sup>73</sup> The Ni(OH)<sub>2</sub>/NF composites have also been prepared by chemical bath deposition.<sup>74</sup> The spike-piece-structured Ni(OH)<sub>2</sub> multilayer nanoplate arrays on nickel foam are directly synthesized by a facile hydrothermal method, which showed high-performance for energy storage.<sup>75</sup> The Ni(OH)<sub>2</sub> nanoflake arrays on Ni foam was fabricated as a binder-free electrode material for high performance supercapacitors.<sup>76</sup> Zhao et al. firstly reported the synthesis of Ni(OH)<sub>2</sub> nanoflakes on Ni micro/nanofibers and the corresponding applications of supercapacitors, the SEM image of mesoporous Ni(OH)<sub>2</sub>-Ni nanohybrids is shown in Fig. 6 (a).<sup>77</sup> They have synthesized porous Ni nanowire foams by the calcination of Ni microfibers in Ar gas. The obtained Ni nanowire foams were further oxidized in an alkaline H<sub>2</sub>O<sub>2</sub> aqueous solution under hydrothermal conditions. The high surface area and mesoporous structure of Ni(OH)<sub>2</sub> offered many nanochannels for the ions or electrolytes, the central Ni improved the conductivity of the as-prepared electrode. The specific capacitances of Ni(OH)<sub>2</sub>-Ni nanohybrids derived from the discharge curves at current densities of 1.25 - 12.5 A g<sup>-1</sup> in 3 M KOH electrolytes is shown in Fig. 6 (b). At a low current density of 1.25 A g<sup>-1</sup>, the mesoporous Ni(OH)<sub>2</sub>-Ni nanohybrid electrode showed a capacitance of 1793 F g<sup>-1</sup>. Even when the current density was 12.5 A g<sup>-1</sup>, the values remained as high as 850 F g<sup>-1</sup>.

Su et al. reported an effective and simple approach to coat amorphous Ni(OH)<sub>2</sub> on a Ni metal core.<sup>78</sup> Fig. 5 (a) shows the SEM image of the 3D-nano Ni, the as-prepared samples were composed of numerous well-defined nanoparticles. The external surface of the nanoparticles are ravine-like, and the diameters of the nanoparticles are approximately 100-200 nm. The SEM images of 3D-nano Ni after Ni(OH)<sub>2</sub> electrodeposition are shown in Fig. 5 (c), suggesting the conformal coating of 3D-nano Ni with Ni(OH)<sub>2</sub> film.

The amorphous Ni(OH)<sub>2</sub>@Ni core-shell electrode manifested apparent advantages as follows: firstly, amorphous Ni(OH)<sub>2</sub>@Ni core-shell electrode as 3D array architecture showed high aspect ratio and high interfacial area.<sup>79</sup> Secondly, amorphous Ni(OH)<sub>2</sub> directly grown on 3D-Ni nanoparticles provided abundant express pathways for fast electron transport. Thirdly, electrodeposition occurred without adding any carbon black or binders, resulting in

reduced internal resistance to enhance rate capability.<sup>80</sup> The specific capacitance of 3D Ni(OH)<sub>2</sub>@Ni core-shell hybrid were 2868, 2857, 2587, and 1980 F g<sup>-1</sup> at scan rates of 1, 2, 5, and 10 mV s<sup>-1</sup>, respectively. The specific capacitance still retained 96 % of the initial capacitance after 3000 cycles.

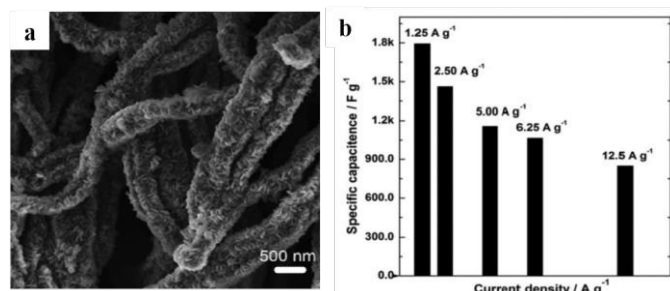


**Fig. 6** SEM images of (a) mesoporous Ni(OH)<sub>2</sub>-Ni nanostructures; (b) specific capacitances of Ni(OH)<sub>2</sub>-Ni nanostructures derived from the discharge curves at current densities of 1.25 - 12.5 A g<sup>-1</sup> in 3 M KOH electrolytes. (a, b) Adapt with the permission from ref. 81, © 2015 The Partner Organisations.

#### 4. Micro/nanostructured nickel sulfide

Among the multitudinous available pseudocapacitive materials, nickel sulfides are subject to intense research in recent years, due to their low cost, ease of fabrication, excellent good electronic conduction, high redox activity.<sup>81-83</sup> Nickel sulfides constitute an important class of metal sulfides, forming many different phases, such as NiS, Ni<sub>3</sub>S<sub>2</sub>, NiS<sub>2</sub>, Ni<sub>3</sub>S<sub>4</sub>, Ni<sub>7</sub>S<sub>6</sub>, Ni<sub>9</sub>S<sub>8</sub>. They have been extensively investigated in recent decades because of their versatile applications in supercapacitors, hydrogenation catalysts, dye-sensitized solar cells and lithium ion batteries.<sup>84,85</sup> Researches on the materials of nickel sulfides indicated that some unique nanostructures can improve the electrochemical properties. Various morphologies of nickel sulfide were synthesized, such as nanotubes,<sup>86</sup> nanorods,<sup>87</sup> core-shell 1D structure,<sup>84</sup> layer-rolled structure,<sup>88</sup> oriented nanostructured thin film,<sup>89</sup> hierarchical flowers,<sup>90</sup> submicrometer hollow microspheres,<sup>91</sup> and so on.

Ni<sub>3</sub>S<sub>2</sub> is one of the most important phases of nickel sulfide, it offers various advantages,<sup>92,93</sup> such as high theoretical capacity, good conductivity and excellent rate performance, which are expected to meet the increasing requirements of energy storage systems. In addition, Ni<sub>3</sub>S<sub>2</sub> is abundant and cheap since it exists in nature as minerals.

Chou et al. successfully synthesized Ni<sub>3</sub>S<sub>2</sub> nanoflakes, then the Ni<sub>3</sub>S<sub>2</sub> nanoflakes were directly electrodeposited on Ni foam and a specific capacitance of 717 F g<sup>-1</sup> at 2 A g<sup>-1</sup> was achieved.<sup>94</sup> However, the electrode was bad in cycling stability, it lost nearly 29 % of the initial capacitance after just 500 cycles. Zhou et al. grew Ni<sub>3</sub>S<sub>2</sub>@Ni(OH)<sub>2</sub>/3DGN (three-dimensional graphene network) on NFs via a one-step hydro-thermal reaction, which exhibited a high capacitance of 1037.5 F g<sup>-1</sup> at 5.1 A g<sup>-1</sup>.<sup>95</sup> Unfortunately, only 38 % of the capacitance was retained as the current density increased from 5.1 A g<sup>-1</sup> to 19.8 A g<sup>-1</sup>.

Huo et al. grew 3D Ni<sub>3</sub>S<sub>2</sub> nanosheet arrays (NSAs) directly on Ni foam with strong adhesion by a facile one-step hydrothermal approach.<sup>96</sup> The as-prepared Ni foam-supported porous Ni<sub>3</sub>S<sub>2</sub> NSAs were endowed with a large electroactive surface area, excellent structural stability, fast electron and ion transport. Additionally, the fabricated asymmetric supercapacitors delivered considerable good long-term stability and energy density. At current densities of 2, 4, 6, 10, 15 and 20 A g<sup>-1</sup>, the specific capacitance values of the Ni<sub>3</sub>S<sub>2</sub> NSAs electrode were calculated to be 1370.4, 1240.8, 1176, 1100, 1020 and 952 F g<sup>-1</sup>, respectively, showing the high specific capacitance and good rate capability. After extending cycling to 1000 cycles, 91.4 % of the capacitance at the 350th cycle can still be maintained, showing its cycling stability. Moreover, the Ni<sub>3</sub>S<sub>2</sub> NSAs electrode also exhibited remarkable electrocatalytic activity towards glucose, including high sensitivity, good selectivity, low detection limit and rapid response. All these impressive measures of performance suggested that the Ni<sub>3</sub>S<sub>2</sub> NSAs is a promising electrode.

Wei et al. successfully synthesized  $\alpha$ -NiS and  $\beta$ -NiS hollow spheres via Kirkendall effect under different hydrothermal conditions. The morphology of the as-prepared  $\alpha$ -NiS and  $\beta$ -NiS samples are shown in Fig. 7(a, b).<sup>97</sup> The obtained  $\alpha$ -NiS and  $\beta$ -NiS hollow spheres were used as electrode materials for supercapacitors. The  $\alpha$ -NiS hollow sphere electrode exhibited large specific capacitance (562.3 F g<sup>-1</sup> at 0.60 A g<sup>-1</sup>) and good cycling property (maintaining about 97.5 % at 2.4 A g<sup>-1</sup> after 1000 cycles).<sup>95</sup>

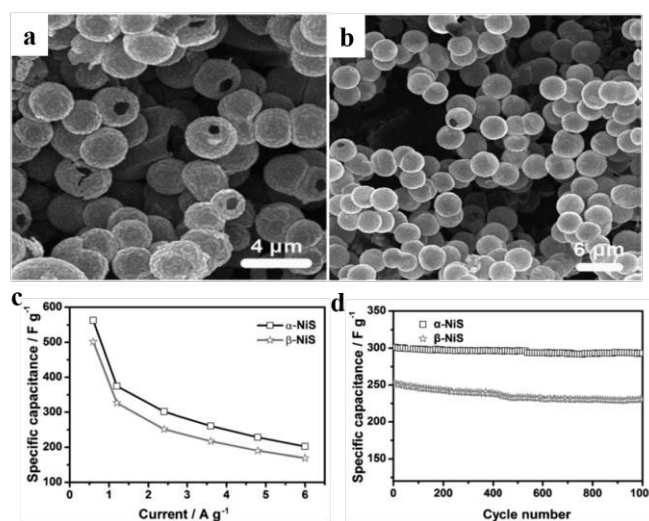


**Fig. 7** (a) SEM image of  $\alpha$ -NiS hollow spheres; (b) SEM image of  $\beta$ -NiS hollow spheres; (c) The specific capacitances calculated from the discharging curves at different current densities; (d) Plots of the specific capacitance as a function of cycle number at a current density of 2.4 A g<sup>-1</sup>. Adapted with permission from ref. 97, © 2015 Wiley.

#### 5. Nickel phosphides and phosphates

Transition metal phosphites have metalloid properties, they have attracted intense attention because of their microporous structures and superior electrical conductivity, catalytic, magnetic, and optical properties.<sup>98-104</sup> Among metal phosphides, nickel phosphides have attracted much interest because they contain a number of phases, remarkable properties and potential applications.<sup>105-108</sup> Nickel

phosphides were synthesized through the reduction of phosphinates and phosphates, high temperatures solid state metathesis, low-temperature solvothermal methods, and so on.<sup>109–114</sup>

The synthesis of transition metal phosphites with well-controlled size and morphology have great significance. Many efforts have been focused on the preparation of nickel phosphate/phosphite micro/nanostructures.<sup>115–117</sup>

Wang et al. prepared amorphous Ni-P by a facile solvothermal method, which served as electrode materials for supercapacitors.<sup>118</sup> Fig. 8 (a) shows us the SEM image of Ni-P product. The TEM image (Fig. 8b) of Ni-P material shows that the equivalent diameter of the as-made Ni-P is about 50–100 nm. As shown in Fig. 8 (c), the specific capacitances were 1597.5 F g<sup>-1</sup>, 1338.75 F g<sup>-1</sup>, 1119 F g<sup>-1</sup>, 964 F g<sup>-1</sup>, and 800 F g<sup>-1</sup> at current densities of 0.5 A g<sup>-1</sup>, 1 A g<sup>-1</sup>, 2 A g<sup>-1</sup>, 4 A g<sup>-1</sup>, and 8 A g<sup>-1</sup>, respectively. In addition, by using Ni-P and activated carbon (AC) as the positive and negative electrode, an asymmetric supercapacitor device was successfully assembled, which can be cycled reversibly in the voltage region of 0–1.6V, offering a high energy density of 29.2 Wh kg<sup>-1</sup> at a power density of 400 W kg<sup>-1</sup>, even operated at a high power density of 8 kW kg<sup>-1</sup> with an energy density of 11.8 Wh kg<sup>-1</sup>. Fig. 8 (d) revealed the cycle performance of the amorphous Ni-P measured at a current density of 4 A g<sup>-1</sup>. The capacitance lost 26.2% during the first 100 cycles, then a slow loss of 3% was observed from 100 to 1000 cycles, showing a relatively good stability.

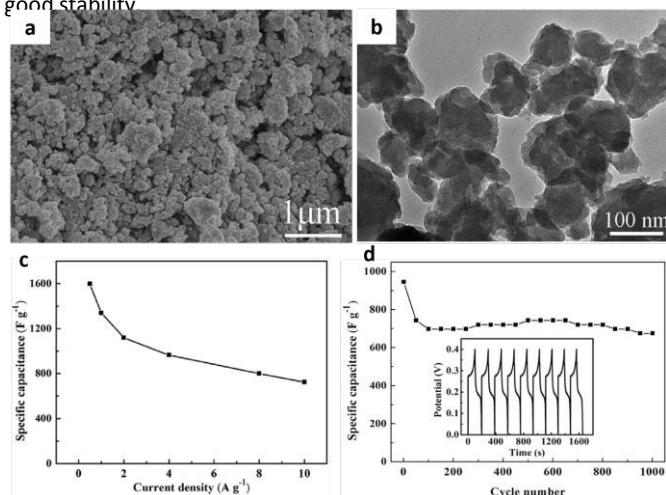


**Fig. 8** (a) SEM image of Ni-P; (b) TEM image of Ni-P; (c) Specific capacitance of the asymmetric capacitor as a function of current density based on the charge-discharge tests curves; (d) The electrochemical stability tests curves of Ni-P at a current density of 4 A g<sup>-1</sup>.

Ni<sub>2</sub>P particles coated with amorphous Ni have been reported to be excellent pseudocapacitive materials,<sup>119</sup> whose specific capacitance reached 1115 F g<sup>-1</sup> at a current density of 2 A g<sup>-1</sup>. The outstanding performance of the Ni<sub>2</sub>P/Ni composites was mainly due to the Ni coating. Gao et al. prepared microporous nickel phosphite (Ni<sub>11</sub>(HPO<sub>3</sub>)<sub>8</sub>(OH)<sub>6</sub>) nanocrystals by a hydrothermal method, which were successfully applied as a positive electrode in a flexible all solid-state asymmetric supercapacitors.<sup>120</sup> The SEM images of the Ni<sub>11</sub>(HPO<sub>3</sub>)<sub>8</sub>(OH)<sub>6</sub> nanocrystals are shown in Fig. 9 (e, f). The supercapacitor achieved a maximum energy density of 0.45 mWh

cm<sup>-3</sup>, and the device performance remained efficient for 10000 cycles.

Zhao et al.<sup>121</sup> successfully synthesized mesoporous uniform ammonium nickel phosphate hydrate nanostructures by a one-pot hydrothermal method. The materials possess high surface area (418 m<sup>2</sup> g<sup>-1</sup>) and tunable structures. As a supercapacitors electrode, it exhibited good performance with a specific capacitance of 1072 F g<sup>-1</sup> in 3.0 M KOH, at a current density of 1.50 A g<sup>-1</sup>, and it remained 95.0 % of initial specific capacitance after 3000 cycles.

Pang et al. successfully synthesized nickel phosphite (Ni<sub>11</sub>(HPO<sub>3</sub>)<sub>8</sub>(OH)<sub>6</sub>) hexagonal polyhedrons under hydrothermal conditions. The SEM images of the hexagonal polyhedrons are shown in Fig. 9 (c, d). The Ni<sub>11</sub>(HPO<sub>3</sub>)<sub>8</sub>(OH)<sub>6</sub> hexagonal polyhedrons were successfully applied as electrochemical supercapacitors electrode materials, which showed a specific capacitance of 295 F g<sup>-1</sup> at 0.625 A g<sup>-1</sup>, and maintained about 99.3 % at 0.625 A g<sup>-1</sup> after 1000 cycles.<sup>122</sup>

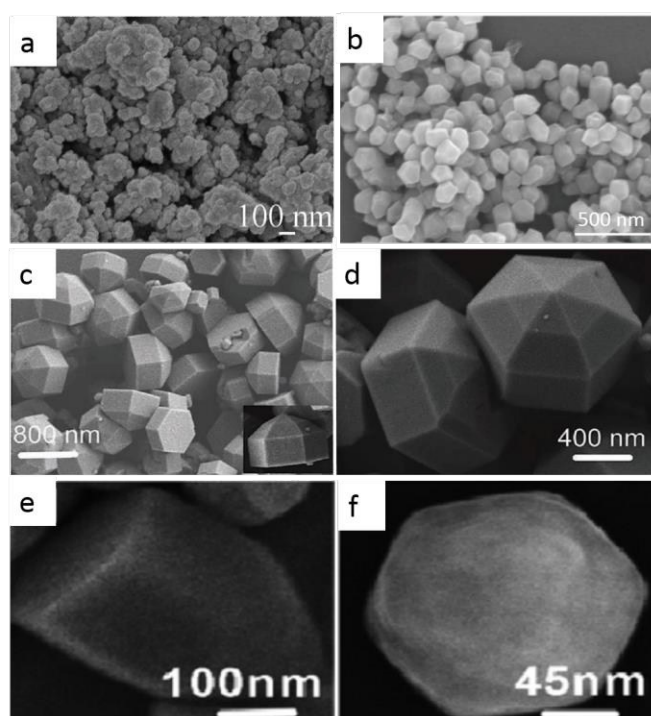


**Fig. 9** SEM images of (a) Ni-P product; (b) Ni<sub>2</sub>P; (c, d) FE-SEM images of Ni<sub>11</sub>(HPO<sub>3</sub>)<sub>8</sub>(OH)<sub>6</sub> hexagonal polyhedrons samples; (e, f) Microporous Ni<sub>11</sub>(HPO<sub>3</sub>)<sub>8</sub>(OH)<sub>6</sub> nanocrystals. (a) Adapted with permission from ref. 117, © 2014 Elsevier; (b) ref. 119, © The Royal Society of Chemistry 2013; (c, d) ref. 122, © 2013 WILEY; (e, f) ref. 120, ©2014 The Royal Society of Chemistry.

## 6. Nickel based mixed and ternary oxide/sulphide

From the Table 3, we can notably found that the Nickel based mixed and ternary oxide/sulphide materials showed ultra-high capacitance and cycling stability. Of the various pseudocapacitive materials, spinel nickel cobaltite (NiCo<sub>2</sub>O<sub>4</sub>) has been conceived as a promising cost-effective and scalable alternative since it offers many advantages, such as abundant resources, low cost and

environmental friendliness.<sup>123-127</sup> The electronegativity of sulfur is lower than oxygen, replacement of oxygen with sulfur may create a more flexible structure, preventing the structure disintegration and making it easy for electrons to transport,<sup>128</sup> which is beneficial to electrochemical performances. Recently, metallic double hydroxides have attracted increasing attention as promising pseudocapacitive materials. Many efforts have been applied in building various special nanostructures to enhance the electrochemical property. For example, Zhou et al. fabricated doughnut-like Ni(OH)<sub>2</sub>-Co(OH)<sub>2</sub> by combination of hydrothermal with chemical deposition approach. The electrode delivered superior electrochemical performance with the specific capacitance of 1398 F g<sup>-1</sup> at the current of 20 A g<sup>-1</sup> and 2193 F g<sup>-1</sup> at the current of 2 A g<sup>-1</sup>.

**Table 3** The capacity and cycling stability of Nickel based mixed and ternary oxide/sulphide materials

Material	specific capacitor (F g <sup>-1</sup> ) (Low current density/scan rate)	specific capacitor (F g <sup>-1</sup> ) (High current density/scan rate)	Capacity retention (%)
Au-NiO <sup>79</sup>	765 (2 A g <sup>-1</sup> )	619 (20 A g <sup>-1</sup> )	~100 % (1000 cycles, 4 A g <sup>-1</sup> )
NiCo <sub>2</sub> O <sub>4</sub> nanosheets <sup>141</sup>	2010 (2 A g <sup>-1</sup> )	1450 (20 A g <sup>-1</sup> )	94 % (2400 cycles, 2 A g <sup>-1</sup> )
NiCo <sub>2</sub> O <sub>4</sub> nanobelt <sup>143</sup>	1647.6 (1 A g <sup>-1</sup> )	1273.5 (25 A g <sup>-1</sup> )	93.6 % (3000 cycles, 25 A g <sup>-1</sup> )
Ni <sub>0.3</sub> Co <sub>0.7</sub> O <sub>2</sub> hierarchical structures <sup>147</sup>	1931 (5 mv s <sup>-1</sup> )	1254 (100 mv s <sup>-1</sup> )	98.1 % (3000 cycles, 0.625 A g <sup>-1</sup> )
NiCo <sub>2</sub> S <sub>4</sub> NTA <sup>159</sup>	2077.6 (10 mA cm <sup>-2</sup> )	–	79.3% (2000 cycles, 60 mA cm <sup>-2</sup> )
NiCo <sub>2</sub> S <sub>4</sub> ball in ball <sup>161</sup>	1036 (1 A g <sup>-1</sup> )	705 (20 A g <sup>-1</sup> )	87 % (2000 cycles, 5 A g <sup>-1</sup> )
NiCo <sub>2</sub> S <sub>4</sub> nanoparticle <sup>162</sup>	1440 (3 A g <sup>-1</sup> )	730 (50 A g <sup>-1</sup> )	91.7 % (5000 cycles, 3 A g <sup>-1</sup> )
Doughnut-like Ni(OH) <sub>2</sub> -Co(OH) <sub>2</sub> <sup>166</sup>	2193 (2 A g <sup>-1</sup> )	1398 (20 A g <sup>-1</sup> )	84.7 % (1000 cycles, 5 A g <sup>-1</sup> )
Layered Ni(OH) <sub>2</sub> -Co(OH) <sub>2</sub> <sup>172</sup>	2158.7 (2 A g <sup>-1</sup> )	1965.6 (5 A g <sup>-1</sup> )	97.5 % (1500 cycles, 10 A g <sup>-1</sup> )
Cu <sub>0.2</sub> Ni <sub>0.8</sub> O <sup>183</sup>	1955 (1 mv s <sup>-1</sup> )	1542 (50 mv s <sup>-1</sup> )	90 % (1000 cycles, 10 A g <sup>-1</sup> )
Co <sub>3</sub> O <sub>4</sub> @NiMoO <sub>4</sub> <sup>202</sup>	1526 (3 mA cm <sup>-2</sup> )	1099 (30 mA cm <sup>-2</sup> )	70 % (1000 cycles, 15 mA cm <sup>-2</sup> )
NiO-Co <sub>3</sub> (VO <sub>4</sub> ) <sub>2</sub> <sup>215</sup>	1166 (0.5 A g <sup>-1</sup> )	940 (8 A g <sup>-1</sup> )	99 % (5000 cycles, 0.5 A g <sup>-1</sup> )

### 6.1 Nickel-Cobalt oxides

Of the various pseudocapacitive materials, spinel nickel cobaltite (NiCo<sub>2</sub>O<sub>4</sub>) has been conceived as a promising cost-effective and scalable alternative since it offers many advantages, such as abundant resources, low cost and environmental friendliness.<sup>123-127</sup> It is reported that spinel NiCo<sub>2</sub>O<sub>4</sub> (NCO) possessed much better electrical conductivity, at least two orders of magnitude higher electrochemical activity than nickel oxides or cobalt oxides.<sup>129,130</sup> Therefore, it is expected to offer richer redox reactions than the monometallic nickel oxides and cobalt oxides. Synthesizing NCO with rationally designed morphology and nanoscale structure provided one of the most feasible ways to create high-performance ECs. Currently, some researches have been carried out to prepare different NCO nanostructures with good electrochemical performances, including nanoflowers,<sup>131</sup> nanoparticles,<sup>132,133</sup> nanoneedles,<sup>134,135</sup> nanoflakes,<sup>136-138</sup> nanowires,<sup>139,140</sup> and various wet-chemical techniques have been used, such as sol-gel methods, hydrothermal, or solvothermal methods.

Yuan et al. fabricated a three-dimensional electrode by growing ultrathin mesoporous NCO nanosheets on Ni foam with strong adhesion for high-performance electrochemical capacitors.<sup>141</sup> The synthesis involved two steps, the co-electrodeposition of a bimetallic (Ni, Co) hydroxide precursor on a Ni foam and succedent thermal transformation to spinel mesoporous NCO. The Ni foam-supported ultrathin mesoporous NCO nanosheets electrode exhibited excellent pseudocapacitance of 2010, 1859, 1694, 1596 and 1450 F g<sup>-1</sup> at current densities of 2, 4, 8, 12 and 20 A g<sup>-1</sup>, respectively. This suggested that about 28 % of the capacitance was lost when the charge-discharge rate increased from 2 to 20 A g<sup>-1</sup>.

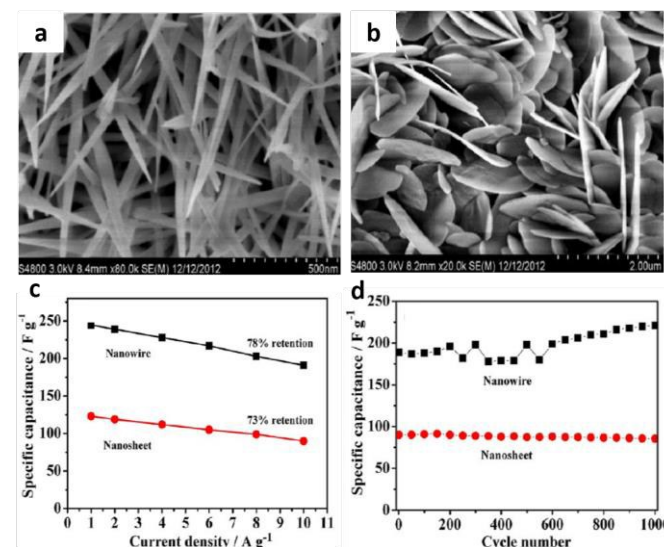


**Fig. 10** FESEM images of the NCO (a) nanowire (b) nanosheet growing on carbon cloth, (c) capacitances versus current densities, and (d) variation of capacitance with cycle number at 10 A g<sup>-1</sup> of the Adapt the permission from ref. 142, © 2013 American Chemical Society.

In order to investigate which nanostructure is the most profitable for capacitive energy storage applications, Wang et al. synthesised nanostructured NCO/carbon cloth electrodes with two different morphologies: the Nanowire and Nano-sheet NCO/Carbon (as shown in Fig. 10 (a, b)).<sup>142</sup> Two steps are involved in the synthesis strategy, a hydrothermal process of mixed metal precursors (Ni, Co) and subsequently a calcination process in air atmosphere. Through galvanostatic charge-discharge, the specific capacitance were calculated and shown in Fig. 10 (c, d). The specific capacitance of the NCO nanowire were 245, 239, 228, 217, 203, 191 F g<sup>-1</sup> at current density of 1, 2, 4, 6, 8, 10 A g<sup>-1</sup>, the capacitance retention was 78 %. In contrast, the specific capacitance of the NCO nanosheet were 123, 119, 112, 105, 99, 90 F g<sup>-1</sup> at 1, 2, 4, 6, 8, 10 A g<sup>-1</sup>, the capacitance retention was 73 %. The results showed that the nanowire morphology exhibited higher specific capacitance and better capacitance retention. The pseudocapacitive difference was related to the surface area and pore structure of NCO nanocrystals. This comparison among different morphologies revealed a process-structure-property relationship in electrochemical energy storage.

Stimulated by the high electrochemical performance of the 1D electrospun materials, Li et al. demonstrated a simple technique of

single-nozzle electrospinning combined with calcination to fabricate ternary 1D NCO nanomaterials. The uniqueness of this strategy was the morphologies of the 1D NCO nanostructures could be tuned by adjusting the precursor concentration. They successfully synthesized NCO-Nanofibers and NCO-Nanobelts, the SEM images are shown in Fig. 11 (a, b). The precursor concentration was critical for formation porous NCO nanotubes, the unique configuration of porous NCO nanotubes facilitated fast ion and electron transport, also alleviated the volume changes during  $\text{OH}^-$  ion insertion/extraction processes. The calculated specific capacitances of NCO-NTs were 1647.6, 1541.2, 1460.3, 1328.3, and 1273.5  $\text{F g}^{-1}$ , at a discharge current densities of 1, 2.5, 5, 10 and 25  $\text{A g}^{-1}$ , respectively. It demonstrated that the novel NCO-NT electrode manifested a high specific capacitance, 77.3 % capacity retention at 25  $\text{A g}^{-1}$  showed its excellent rate capability, 6.4 % lost after 3000 cycles proved its outstanding cycling stability. So, the NCO-NTs can serve as advanced electrode materials for supercapacitors.<sup>143</sup> When the synthesized  $\text{Ni}_{0.5}\text{Co}_{1.5}(\text{OH})_2\text{CO}_3$  nanowire arrays (NWAs) were immersed in 6 M NaOH for 6 to 18 h, small and thin nanoplatelets were developed on the surface of the NWAs. The hierarchical nanowire@nanoplatelet arrays showed high areal capacitance and specific capacitance of 9.59  $\text{F cm}^{-2}$ , 928.4  $\text{F g}^{-1}$  at 5  $\text{mA cm}^{-2}$ , at least seven times larger than those of the pristine NWAs. In addition, it retained 81 % of the highest capacitance at a high current density of 50  $\text{mA cm}^{-2}$ , exhibited good rate capability.<sup>144</sup>

Pang et al. reported a facile synthesis of mesoporous nickel cobalt oxide ( $\text{Ni}_{0.3}\text{Co}_{2.7}\text{O}_4$ ) hierarchical structures with excellent electrochemical performance for SCs.<sup>147</sup> They synthesized nickel cobalt oxalate hydrate ( $\text{Ni}_{0.1}\text{Co}_{0.9}\text{C}_2\text{O}_4 \cdot n\text{H}_2\text{O}$ ) as the precursor, following by a controlled calcination process to synthesize mixed mesoporous nickel cobalt oxide hierarchical structures. The  $\text{Ni}_{0.1}\text{Co}_{0.9}\text{C}_2\text{O}_4 \cdot n\text{H}_2\text{O}$  precursor was heated from room temperature to 400, 450, 500  $^\circ\text{C}$  for 10 min with a heating rate of 1  $^\circ\text{C min}^{-1}$ , the obtained product were denoted as P1, P2, P3, respectively. It was found that the p1 samples possessed more abundant mesopores and higher BET surface area (44, 35, 28  $\text{m}^2 \text{g}^{-1}$  for P1, P2, and P3, respectively), and exhibited excellent supercapacitive performance in aqueous alkaline electrolytes. Though the CV test, high specific capacitance of 1931, 1665, and 1478  $\text{F g}^{-1}$  were obtained at a scan rate of 5  $\text{mV s}^{-1}$  for P1, P2 and P3, respectively. And the mesoporous  $\text{Ni}_{0.3}\text{Co}_{2.7}\text{O}_4$  hierarchical structures showed a remarkable capacitance of 1254, 1037 and 1164  $\text{F g}^{-1}$  at a high scan rate of 100  $\text{mV s}^{-1}$  for P1, P2 and P3, respectively. Similar to the results obtained from CV tests, it also exhibited high specific capacitance and excellent rate capability. The samples deliver a high capacitance of 960, 834, 713  $\text{F g}^{-1}$  at a relatively low current density of 0.625  $\text{A g}^{-1}$  for P1, P2, P3, respectively. Even when the current density was increased to 6.25  $\text{A g}^{-1}$ , the values remained as 805, 706, 652  $\text{F g}^{-1}$  for P1, P2, P3, respectively, showing an remarkable cycling stability. The exceptional electrochemical performance were likely due to the desirable composition and the unique hierarchical mesoporous architectures.

## 6.2 Nickel-Cobalt sulfides

The electronegativity of sulfur is lower than oxygen, replacement of oxygen with sulfur may create a more flexible structure, preventing the structure disintegration and making it easy for electrons to

transport,<sup>128</sup> which is beneficial to electrochemical performances. And due to the lower band gap, ternary  $\text{NiCo}_2\text{S}_4$  possess an electric conductivity  $\sim 100$  times than that of NCO<sup>148-151</sup> although NCO has been reported to possess good electric conductivity.<sup>152</sup> Recently, many researchers explored the use of nickel cobalt sulphide in the application of ECs.<sup>153-155</sup>

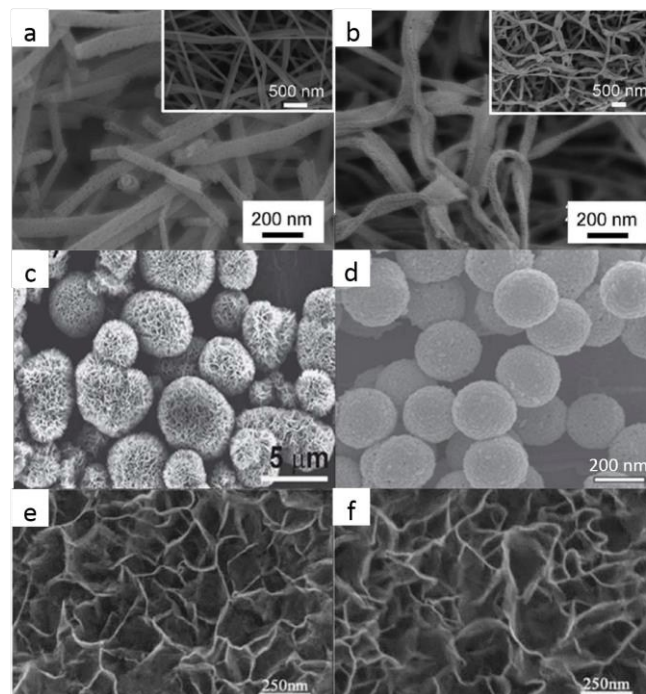


**Fig. 11** SEM images of (a) NCO-Nanofibers and (b) NCO-Nanobelts; (c) hybrid  $\text{NiO}/\text{Co}_3\text{O}_4$ ; (d)  $\text{NiCo}_2\text{S}_4$  ball-in-ball hollow spheres; (e)  $\text{Ni}_{0.7}\text{Co}$  oxide, (f)  $\text{Ni}_{0.78}\text{Co}_{0.22}$  oxide. (a, b) Adapt the permission from ref. 143, © 2013 Wiley; (c) ref. 145, © 2013 The Royal Society of Chemistry; (d) ref. 161, © 2015 Macmillan; (e, f) ref. 146, © 2013 The Royal Society of Chemistry.

Jiang et al. reported the highly conductive  $\text{NiCo}_2\text{S}_4$  urchin-like nanostructures, which exhibited a high capacitance of 1062  $\text{F g}^{-1}$  at 4  $\text{A g}^{-1}$ .<sup>148</sup> Lou et al. synthesized  $\text{NiCo}_2\text{S}_4$  hollow prisms, which delivered a high capacitance of 834.4  $\text{F g}^{-1}$  at 2  $\text{A g}^{-1}$ .<sup>150</sup> Among various nanostructures, the hollow tubular nanostructures have attracted extensive research interests.<sup>156,157</sup> Recently, Pu et al. reported the growth of  $\text{NiCo}_2\text{S}_4$  nanotubes arrays (NTAs) on nickel foam for supercapacitors, which displayed a low specific capacitance of 783  $\text{F g}^{-1}$  at a current density of 4  $\text{A g}^{-1}$ .<sup>158</sup> Wan et al. reported the  $\text{NiCo}_2\text{S}_4$  porous nanotubes for supercapacitors, which showed a low specific capacitance of 933  $\text{F g}^{-1}$  at 1  $\text{A g}^{-1}$ .<sup>156</sup>

Cai et al. successfully synthesized the desirable  $\text{NiCo}_2\text{S}_4$  NTAs grown on nickel foam substrate through a facile two-step hydrothermal method.<sup>157</sup> Fig. 12 (c) clearly shows that the whole process involves two steps: (1) surfactant-assisted hydrothermal growth of NiCo- precursor NWAs on nickel foam as previously reported by Zhang et al.,<sup>158</sup> (2) using  $\text{Na}_2\text{S}$  as the sulfur source, the NiCo- precursor NWAs are transformed into  $\text{NiCo}_2\text{S}_4$  NTAs via a simple and facile hydrothermal method based on the Kirkendall

effect. Fig. 12 (a, b) show SEM images of the  $\text{NiCo}_2\text{S}_4$  NTAs and NCO NWAs on nickel foam, respectively.

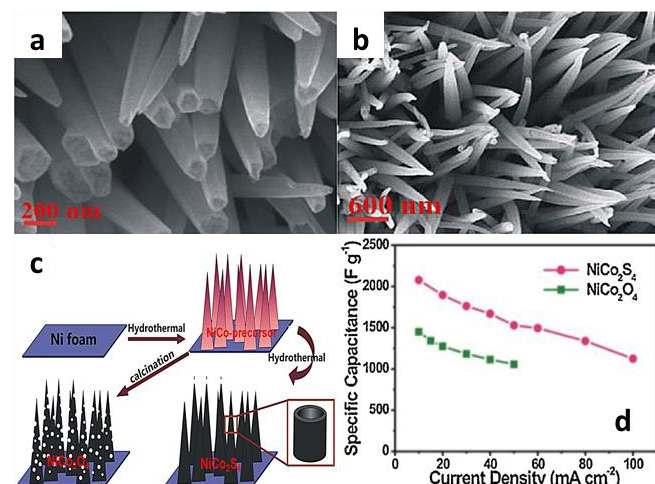


**Fig. 12** (a,b) SEM images of the  $\text{NiCo}_2\text{S}_4$  NTAs / NCO NWAs on nickel foam; (c) Schematic illustrations of the growth of  $\text{NiCo}_2\text{S}_4$  NTAs and NCO NWAs on nickel foam; (d) the calculated capacitance as a function of current density according to the charge and discharge curves. Adapt the permission from ref. 159, © 2014 Elsevier.

This electrode design avoided the use of polymer binder and conducting additives, improving the utilization of the electrode materials even at a high massloading. In addition, the  $\text{NiCo}_2\text{S}_4$  NTAs grown on nickel foam are synthesized with the help of surfactant, which avoided for mingdense structure and ensured larger surface areas for Faradaic reactions.<sup>160</sup> Pressively, the  $\text{NiCo}_2\text{S}_4$  NTA electrode exhibited much enhanced electrochemical performance than the mesoporous NCO NWA electrode, which held great promise for high-performance supercapacitors applications. The as-prepared  $\text{NiCo}_2\text{S}_4$  NTA electrode exhibited significantly electrochemical performance comparing with the mesoporous NCO NWA electrode. As shown in Fig. 12 (d), at a high current density of  $10 \text{ mA cm}^{-2}$ , the capacitance of the  $\text{NiCo}_2\text{S}_4$  NTA electrode were as high as  $2077.6 \text{ F g}^{-1}$ , which was much higher than  $1451.6 \text{ F g}^{-1}$  of the mesoporous NCO NWA electrode.

Shen et al. reported a facile anion exchange method to synthesize a ball-in-ball hollow structure of ternary nickel cobalt sulfide ( $\text{NiCo}_2\text{S}_4$ ), the SEM image is shown in Fig. 11 (d).<sup>161</sup> Uniform nickel cobalt glycerate solid spheres were first synthesized as the precursor and subsequently chemically transformed into nickel cobalt sulfide ball-in-ball hollow spheres. The procedure involves a facile solvothermal synthesis of metal-glycerate solid spheres and sulfidation in the presence of thioacetamide (TAA) to form  $\text{NiCo}_2\text{S}_4$  ball-in-ball hollow spheres. When it was used as electrode materials for electrochemical capacitors, a maximum specific capacitance reached  $1036 \text{ F g}^{-1}$  at a discharge current density of  $1 \text{ A g}^{-1}$ , and the corresponding volumetric capacitance was  $518 \text{ F cm}^{-3}$ . The specific capacitance of the  $\text{NiCo}_2\text{S}_4$  electrode kept a high value of  $705 \text{ F g}^{-1}$  at  $20 \text{ A g}^{-1}$ , about 68.1 % of the capacitance was retained when the current density increased from 1 to  $20 \text{ A g}^{-1}$ .

Zhu et al. adopted a solvothermal method to synthesize uniform mesoporous  $\text{NiCo}_2\text{S}_4$  nanoparticles.<sup>162</sup> The as-obtained  $\text{NiCo}_2\text{S}_4$  nanoparticles demonstrate excellent electrochemical performances, electrochemical results showed ultrahigh specific

capacitance of  $1440 \text{ F g}^{-1}$  at  $3 \text{ A g}^{-1}$  after 250 cycles, and exceptional rate capability of 75.1 % capacity remained from 2 to  $50 \text{ A g}^{-1}$ . Moreover, asymmetric supercapacitors were obtained by using the AC and  $\text{NiCo}_2\text{S}_4$  as the negative and positive electrodes, respectively, displaying high energy density and good electrochemical cycling stability. The energy density was  $28.3 \text{ Wh kg}^{-1}$  at the power density of  $245 \text{ W kg}^{-1}$ , 91.7 % of the initial capacity remained at  $3 \text{ A g}^{-1}$  over 5000 cycles.

### 6.3 Nickel/Cobalt layered double hydroxides

Metallic double hydroxides have attracted increasing attention as promising pseudocapacitive materials because of their large specific capacitance, rich reserve, low price and natural friendliness.<sup>163-165</sup> However, the unsatisfactory structural stability and conductivity seriously restrict their practical applications in high-performance supercapacitors.

These results are inspiring, but a relatively low utilization rate of electroactive materials still limits the development of supercapacitors. To endow nanostructures with more electroactive sites, hollow nano/microstructures arouse great interest. The unique structure possesses many advantages with large surface area, preferable electrolyte accesses and favourable charge transfer, thus leading to an enhanced specific capacitance.<sup>168,169</sup> Owing to the largest surface area, hollow Ni/Al double hydroxides offers the best pseudocapacitance performance.

Chen et al. used MOF as the template for the synthesis of hollow nickel/cobalt layered double hydroxides (Ni/Co-LDH) nanocage, which showed ultrahigh BET area giving high specific capacitance.<sup>167</sup> Wei et al. reported a facile method for the fabrication of Ni/Al double hydroxide microspheres with core-shell, yolk-shell and hollow interior nanostructures.<sup>170</sup> Chen et al. fabricated an urchin-like  $\text{Ni}(\text{OH})_2\text{-Co}(\text{OH})_2$  hollow microspheres by microwave-incorporated hydrothermal method, exhibiting a specific capacitance of  $2164 \text{ F g}^{-1}$  at the current of  $1 \text{ A g}^{-1}$ .<sup>171</sup> These template synthesis methods of layered double hydroxides (LDH) hollow microspheres were very complex, energy-consuming, time-consuming and difficult to use in scale production.

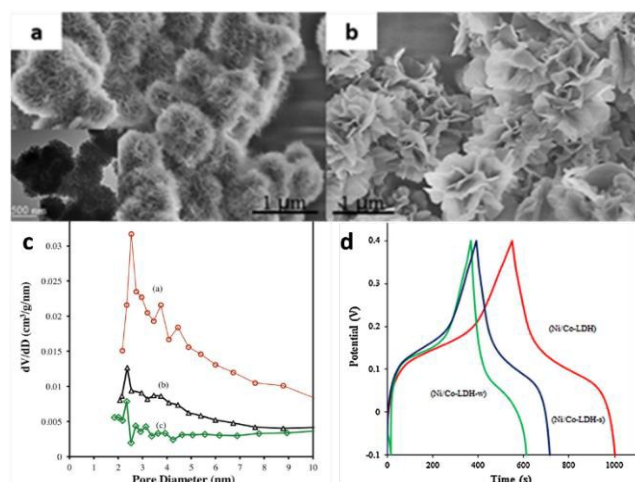


**Fig. 13** SEM (a) and TEM (inset) image of Ni/Co-LDH-s, and SEM (b) image of Ni/Co-LDH-w; (c) pore size distributions of Ni/Co-LDH (a), Ni/Co-LDH-s (b) and Ni/Co-LDH-w (c); (d) First charging/discharging

curves of those electrodes at the current density of  $2 \text{ A g}^{-1}$ . Adapt the permission from ref. 172, © 2014 Elsevier.

Tao et al. developed a new template synthesis of Ni/Co-LDH with hydrangea-like morphology using  $\text{SiO}_2$  nanosphere as sacrificial template. For comparison, two kinds of Ni/Co-LDH samples were prepared using the above procedure, but with urea as an adsorbent alkali source or without  $\text{SiO}_2$  template, which were named to Ni/Co-LDH-s and Ni/Co-LDH-w (shown in Fig. 13 (a, b)). This new synthesis method was no use of any oxidant and steps for removal of the template, it achieved a perfect match between removal rate of template and generation rate of Ni/Co-LDH nanoflakes.<sup>172</sup>

The as-prepared Ni/Co-LDH showed a homogeneous 3D structure with well-defined hydrangea-like exterior and hollow interior, and provided excellent electrochemical performance for supercapacitors. The calculated specific capacitance values were 2106.8, 2053.8, 2019.8, 1965.6  $\text{F g}^{-1}$  at 2, 3, 4 and 5  $\text{A g}^{-1}$ , respectively, 93.3 % capacitance were remained when the current increased from 2 to 5  $\text{A g}^{-1}$ . In addition, charging/discharging curves of Ni/Co-LDH, Ni/Co-LDH-s and Ni/Co-LDH-w at 2  $\text{A g}^{-1}$  are shown in Fig. 13 (d). The corresponding capacitive values were calculated to be 2106.8, 1454.5 and 1154.5  $\text{F g}^{-1}$ , respectively. The Ni/Co-LDH showed the best specific capacitance among them, it was attributed to the unique architecture with hollow interior and ultrathin nanostructure, which were beneficial for electrolyte access and penetration. The as-prepared Ni/Co-LDH showed excellent electrochemical property, deserving wide application as the electrode materials in high-performance supercapacitors.

#### 6.4 Other nickel-related mixed oxides

##### 6.4.1 Au-NiO hierarchical structures

The rate performance of NiO nanostructures is limited due to intrinsically poor electrical conductivity. Therefore, some binary composites of NiO materials were explored with some improvement in rate performance.<sup>173-176</sup> Because of the reduction of charge-transfer resistance, compounding conductive Au and Ag on metal oxides pseudo-capacitor electrodes was taken out to improve rate performance.<sup>72,177</sup> Qu et al. presented a simple solution method to synthesize Au-decorated hierarchical NiO nanostructures (Au-NiO).<sup>178</sup> As a pseudo-capacitor electrode, Au-NiO exhibited remarkable cycling ability and excellent rate capability, which were superior to previously reported NiO based electrode materials.<sup>173-176,179</sup> The specific capacitances of bare NiO electrode at current densities of 2, 4, 8, 10 and 20  $\text{A g}^{-1}$  were 475, 362, 304, 265 and 216  $\text{F g}^{-1}$ , respectively. Nonetheless, the Au-NiO electrode exhibited meaningful specific capacitances of 765, 692, 644, 623 and 619  $\text{F g}^{-1}$  at current densities of 2, 4, 8, 10 and 20  $\text{A g}^{-1}$ , respectively.

##### 6.4.2 Nickel copper oxide nanowires

Copper oxide is low-cost, non-toxic, easily-producible and readily-storable,<sup>180-183</sup> the capacitance of copper oxide is very low (under 600  $\text{F g}^{-1}$ ).<sup>180,181</sup> To the best of our knowledge, reports on nickel copper oxide are rare except one paper studying Ni-Cu-Co oxyhydroxide.<sup>182</sup> Zhang et al. successfully synthesized nickel copper oxide nanowires on the current collector via a simple and industrially compatible route.<sup>183</sup> They expected those samples could be high-performance and low-cost candidate for supercapacitors application, therefore two strategies were utilized. First, instead of

combining metal oxides that have good supercapacitors performance such as Co, Mn and Ru with nickel oxide, copper is chosen, which is adjacent to nickel in the periodic table. Second, the binder-free method was adopted to grow active materials directly on the current collector, avoiding tedious preparation and achieving good mechanical adhesion and good contact. They synthesized pristine NiO and CuO with the same method. The prepared  $\text{Cu}_{0.2}\text{Ni}_{0.8}\text{O}$  delivered high capacitance and excellent cycle life. The capacitance was 1955  $\text{F g}^{-1}$  at 1  $\text{mV s}^{-1}$ , which still maintained 1542  $\text{F g}^{-1}$  at 50  $\text{mV s}^{-1}$ , furthermore, it retained 90 % after 1000 cycles at 10  $\text{A g}^{-1}$ .

##### 6.4.3 Three dimensional hybrid $\text{Co}_3\text{O}_4@/\text{NiMoO}_4$ nanosheet arrays

Up to now, the synthesis of metal oxides NSAs were generally implemented by two approaches: electro-deposition and hydrothermal synthesis.<sup>184-188</sup> In contrast to electro-deposition, active materials obtained by hydrothermal synthesis provide large-scale and uniform NSAs with numerous large channels, which would facilitate the design and fabrication of 3D hybrid nanostructures.<sup>184,189-192</sup> However, the capacitance values of 2D building blocks obtained by hydrothermal synthesis are still limited.<sup>193-196</sup> Till now, the reported electrode materials based on  $\text{NiMoO}_4$  were usually made by slurry-coating method, where the involved carbon current collector and polymer binders would seriously depress the pseudo-capacitive performance.<sup>197-201</sup>

Hong et al. prepared uniform 2D  $\text{Co}_3\text{O}_4$ -based building blocks through a facile chemical etching assistant approach, and used the products to construct a binder-free electrode with hybrid nanostructured  $\text{Co}_3\text{O}_4@/\text{NiMoO}_4$  directly grown on Ni foam.<sup>202</sup> The TEM image of hybrid  $\text{Co}_3\text{O}_4@/\text{NiMoO}_4$  NSAs is shown in Fig. 14 (a), the as-synthesized 3D  $\text{Co}_3\text{O}_4@/\text{NiMoO}_4$  electrode exhibited a

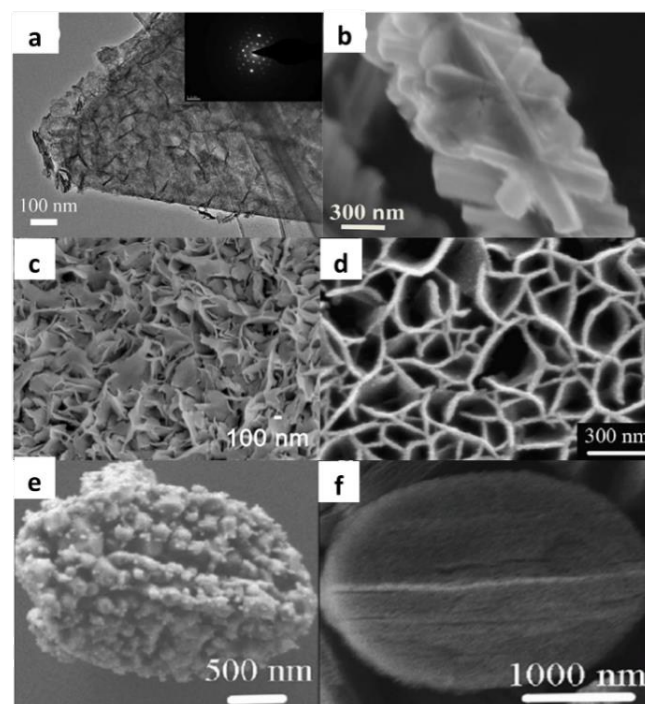


**Fig. 14** (a) TEM image of hybrid  $\text{Co}_3\text{O}_4@/\text{NiMoO}_4$  NSAs; SEM images of (b) the NCO-MnO<sub>2</sub> NWs; (c) NiO-Co<sub>3</sub>(VO<sub>4</sub>)<sub>2</sub> nanocomposite grown on Ni foam; (d) NiO/Ag composite film; (e, f) porous ZnO-NiO composites. (a) Adapt the permission from ref. 202; (b) ref. 187; (c)

ref. 229, © 2014 Elsevier; (d) ref. 188, © 2010 Elsevier; (e, f) ref. 32; © 2012 The Royal Society of Chemistry.

specific capacitance of  $1526 \text{ F g}^{-1}$  at  $3 \text{ mA cm}^{-2}$ , and 72 % capacity were retained at  $30 \text{ mA cm}^{-2}$ . The ASC values were calculated to 2.67, 2.58, 2.49, 2.35, 2.24, 2.12 and  $1.92 \text{ F cm}^{-2}$  at current densities of 3, 5, 7, 10, 15, 20 and  $30 \text{ mA cm}^{-2}$ , respectively. The capacitance values in this work were superior to those previously reported core/shell nanostructures, such as NCO@MnO<sub>2</sub> NWAs ( $2.244 \text{ F cm}^{-2}$  at  $2 \text{ mA cm}^{-2}$ ),<sup>203</sup> NCO@NCO NSAs ( $2.20 \text{ F cm}^{-2}$  at  $5 \text{ mA cm}^{-2}$ ),<sup>191</sup> Co<sub>3</sub>O<sub>4</sub>@NiO NWAs ( $1.35 \text{ F cm}^{-2}$  at  $6 \text{ mA cm}^{-2}$ ),<sup>204</sup> NiMoO<sub>4</sub>·XH<sub>2</sub>O nanorods ( $1136 \text{ F g}^{-1}$  at  $5 \text{ mA cm}^{-2}$ ).<sup>206</sup>

To further evaluate the practical application of this hybrid Co<sub>3</sub>O<sub>4</sub>@NiMoO<sub>4</sub> NSA in electrical energy storage devices, an asymmetric supercapacitor based on this hybrid Co<sub>3</sub>O<sub>4</sub>@NiMoO<sub>4</sub> NSA and activated carbon was fabricated. The asymmetric supercapacitor achieved a specific capacitance of  $121 \text{ F g}^{-1}$  at a current density of  $5 \text{ mA cm}^{-2}$ , and delivered a maximum energy density of  $37.8 \text{ Wh kg}^{-1}$  at a power density of  $482 \text{ W kg}^{-1}$ . The values in this work were higher than those previously reported asymmetric supercapacitors with aqueous electrolytes, such as Ni-Co binary hydroxides couples with chemically reduced graphene ( $26.3 \text{ Wh kg}^{-1}$ ),<sup>207</sup> NCO@MnO<sub>2</sub>//AC ( $35 \text{ Wh kg}^{-1}$ ),<sup>203</sup> Ni-Co sulfides//AC ( $25 \text{ Wh kg}^{-1}$ ).<sup>165</sup> Such charming electrochemical performance presented here implied this hybrid electrode was a promising candidate for practical applications in supercapacitors.

#### 6.4.4 Nickel hexacyanoferrate flower-like nanosheets coated three dimensional porous nickel films

Nickel hexacyanoferrate (NiHCF) is considered to be one of the most promising electrode materials for electrochemical capacitors, which could switch between reduced and oxidized states in neutral electrolyte containing alkali metal cations such as potassium, lithium, and sodium.<sup>208,209</sup> The neutral electrolyte does not easily corrode other components and is much cheaper than the organic electrolyte, but the low electrical conductivity of NiHCF limits the electrochemical performance. Recently, 3D porous micro/nanostructures interconnected metal matrix composite electrodes without binder attract great attention for electrochemical energy storage and conversion, in which the active materials were directly grown on the metal substrate and interconnected with the 3D conductive metal nanostructure scaffold.<sup>145,210,211</sup> Different methods have been developed to fabricate 3D porous metals such as de-alloy, carbon template, H<sub>2</sub> gas bubble dynamic template, polymer template, SiO<sub>2</sub> template, etc.<sup>211-213</sup>

Jiang et al. fabricated flower-like NiHCF nanosheets directly on the 3D porous Ni interconnected current collectors as integrated film electrodes for supercapacitors with neutral electrolyte, the structure and performance of the 3D porous NiHCF/Ni films were investigated.<sup>214</sup> The high magnification SEM images in Fig. 15 (a, b) illustrated that the NiHCF layer consisted of many interconnected flower-like nanosheets with highly porous surface on the 3D porous Ni walls. Fig. 15 (c) shows the relationship between the current density and discharge areal specific capacitance of 3D porous NiHCF/Ni film electrode. When the current density increased to  $1.5 \text{ mA cm}^{-2}$ , it still exhibited a high areal specific capacitance of  $88.6 \text{ mF cm}^{-2}$ . Those excellent electrochemistry performance of 3D porous NiHCF/Ni film electrode might be ascribed to the remarkable 3D hierarchical porous structure feature, and the direct growth of flower-like nanosheets NiHCF on the Ni network without polymer binder.

#### 6.4.5 Three dimensional nanostructured NiO-Co<sub>3</sub>(VO<sub>4</sub>)<sub>2</sub> compounds

The Co<sub>3</sub>(VO<sub>4</sub>)<sub>2</sub> was found to have outstanding electrochemical performance, especially the excellent rate capability and the cycle performance. The 3D nanostructured NiO-Co<sub>3</sub>(VO<sub>4</sub>)<sub>2</sub> compound on nickel foam as a binder-free electrode was fabricated for high-performance ECs by Zhang et al.,<sup>215</sup> the SEM image of NiO-Co<sub>3</sub>(VO<sub>4</sub>)<sub>2</sub> nanocomposite grown on Ni foam is shown in Fig. 14 (c).

They used a facile and scalable strategy to fabricate the 3D nanostructured NiO-Co<sub>3</sub>(VO<sub>4</sub>)<sub>2</sub> compound, which exhibited excellent energy density of  $25.8 \text{ Wh kg}^{-1}$ , high specific capacitance of  $1166 \text{ F g}^{-1}$  at a current density of  $0.5 \text{ A g}^{-1}$ , and perfect cycling stability of more than 99 % retained after 5000 cycles. The intriguing capacitive behavior was ascribed to the unique 3D structure, efficient electrode reaction, nice crystallinity and the synergistic effects of the combined NiO nanowires with the Co<sub>3</sub>(VO<sub>4</sub>)<sub>2</sub> nanoflakes.

## 7. Nickel compound-carbon material composites

To make full use of active materials and achieve high performance, their morphologies are always designed to provide sufficient ion-transport pathways, such as porous or nanosized structures. For example, various nanostructured Ni(OH)<sub>2</sub> including nanoflowers,<sup>216,217</sup> nanoplates<sup>218,219</sup> and hierarchical nanostructures<sup>95,220</sup> have been reported as high-performance

supercapacitors electrode materials. These specially designed nanostructures were valid shorten ion-transport pathways, but the

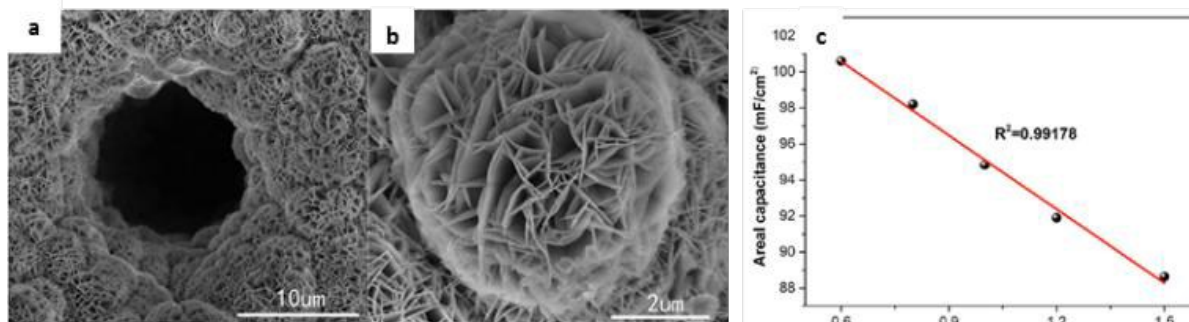


**Fig. 15** (a, b) SEM images of porous Ni films coating NiHCF; (c) the relationship between the current density and discharge specific capacitance of 3D porous NiHCF/Ni film electrode. Adapt the permission from ref. 214, © 2015 Elsevier.

poor electronic conductivities of metal oxides/hydroxides markedly hinder electron transport and decelerate redox reactions, resulting in low capacitances and bad rate capabilities. The most commonly used method for improving their electronic conductivities is to combine them with carbon materials,<sup>221,222</sup> conducting polymers,<sup>223,224</sup> and even current collectors.<sup>204</sup> Carbon materials (including carbon nanotubes, graphene, and activated carbon) are the most frequently used conductive substrates because of their good electronic conductivities, high specific surface areas, and great chemical stabilities. Nevertheless, it is very difficult to directly grow metal oxides/hydroxides on carbon materials, because their surfaces are not compatible. To improve their surface compatibility, oxidative treatments of carbon materials are always necessary, which could introduce oxygen-containing groups facilitating the growth of metal oxides/hydroxides and numerous structural defects on the surfaces of carbon materials.<sup>225</sup>

Recently, Gu et al. synthesised a silicon carbide nanowires@Ni(OH)<sub>2</sub> core-shell structures.<sup>226</sup> By chemical vapor deposition method, silicon carbide (SiC) nanowires were grown on flexible carbon fabric, and Ni(OH)<sub>2</sub> are deposited on the surface of SiC NWs by electrochemical cathodic deposition. The capacitive performance of the as-prepared electrode were calculated based on pure Ni(OH)<sub>2</sub>. A high specific capacitance was 1724 F g<sup>-1</sup> at 2 A g<sup>-1</sup> and the electrode still had a specific capacitance of 1412 F g<sup>-1</sup> at 100 A g<sup>-1</sup>. With the charge/discharge rate of 100 A g<sup>-1</sup>, a high power density of 27.5 kW kg<sup>-1</sup> was achieved and the energy density still remained 59.4 Wh kg<sup>-1</sup>.

### 7.1 Combined with carbon nanotubes

Nickel and cobalt mixed oxides (Ni/Co)O<sub>x</sub> were electrochemically deposited onto CNT films coated-Ni mesh and pristine Ni mesh.<sup>227</sup> The CNT films provided a large surface and interfacial area, in order to prevent the smaller particles merging together after continuouitances of (Ni/Co)O<sub>x</sub> on CNTs-Ni mesh and on Ni mesh were 840 F g<sup>-1</sup> and 475 F g<sup>-1</sup>, respectively. In addition, the presence of CNT films effectively increased the cycling stability. Comparative studies showed that (Ni/Co)O<sub>x</sub>-CNTs (Ni/Co molar ratio 1 : 1) had the best reversibility and capacitance.<sup>228</sup> The specific capacitance of (Ni/Co)O<sub>x</sub>-CNTs was 569 F g<sup>-1</sup>, about 3 times higher than (Ni/Co)O<sub>x</sub> of 193 F g<sup>-1</sup>.

Ma et al. used nickel-coated carbon nanotubes (Ni-CNTs) as conductive substrate for the growth of β-Ni(OH)<sub>2</sub>.<sup>229</sup> First, Ni-CNTs@α-Ni(OH)<sub>2</sub> composites were prepared by a solvothermal reaction at 180 °C, then it was transformed into Ni-CNTs@β-Ni(OH)<sub>2</sub> after a hydrothermal reaction in alkaline solution. The thickness of β-Ni(OH)<sub>2</sub> nanoplates was only few nanometers (~5-10 nm), greatly shortening ion-transport pathways. Benefiting from the nanostructures, as-prepared Ni-CNTs@β-Ni(OH)<sub>2</sub> composites exhibited high specific capacitances (~1807 F g<sup>-1</sup> at 2 A g<sup>-1</sup>, based on the mass of β-Ni(OH)<sub>2</sub>; ~1283 F g<sup>-1</sup> at 2 A g<sup>-1</sup>, based on the total mass of composite), good rate capabilities, and excellent cycling stabilities.

The morphology and content of β-Ni(OH)<sub>2</sub> could be controlled by modulating the ratio of NiCl<sub>2</sub>·6H<sub>2</sub>O to Ni-CNTs. The diameter of Ni-CNTs@β-Ni(OH)<sub>2</sub> rods could be controlled from ~300 to ~500 nm by modulating the ratio of NiCl<sub>2</sub>·6H<sub>2</sub>O to Ni-CNTs, as the SEM

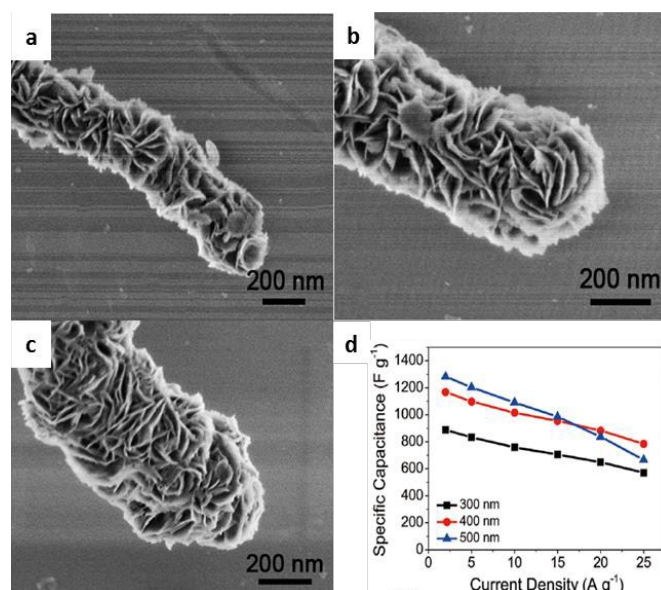


**Fig. 16** SEM images of sample a with an average diameter of (a) ~300 nm; (b) ~400 nm; (c) ~500 nm; (d) Specific capacitances of three Ni-CNTs@β-Ni(OH)<sub>2</sub> samples at different current densities. Adapted with permission from ref. 229, © 2014 American Chemical Society.

images shown in Fig. 16 (a-c), while the content of β-Ni(OH)<sub>2</sub> could be increased from 49 wt % to 71 wt %. Because of the different contents of β-Ni(OH)<sub>2</sub>, three Ni-CNTs@β-Ni(OH)<sub>2</sub> samples showed quite different specific capacitances. As shown in Fig. 16 (d), sample ~500 nm exhibited the highest specific capacitance of ~1283 F g<sup>-1</sup> at 2 A g<sup>-1</sup>, while the specific capacitances of the other two samples were 1168 and 887 F g<sup>-1</sup> at 2 A g<sup>-1</sup>, respectively.

Tang et al. reported an additive-free, nano-architected Ni(OH)<sub>2</sub>/CNT/NF electrode with a related asymmetric supercapacitors.<sup>230</sup> The TEM image of as-deposited Ni(OH)<sub>2</sub>/CNT composites is shown in Fig. 17 (a), the SEM images of Ni(OH)<sub>2</sub>/CNT/NF is shown in Fig. 17 (b). This nano-architected Ni(OH)<sub>2</sub>/CNT/NF electrode was prepared by a facile two-step method. The first step was to prepare the Ni(OH)<sub>2</sub>/CNT/NF electrode, carbon nanotubes (CNTs) were directly grown onto Ni foam via a thermal chemical vapor deposition (CVD) process. The second step was conformal deposition of Ni(OH)<sub>2</sub> onto the CNT layers via chemical bath deposition (CBD) process. The layered graphitic walls of the CNT support can also be clearly seen underneath the Ni(OH)<sub>2</sub> nanoshell.

Fig. 17 (c) shows the CV curves of the CNT/NF substrate, the Ni(OH)<sub>2</sub>/CNT/NF electrode and the Ni(OH)<sub>2</sub>/NF electrode between a potential window of 0 and 0.4 V at a scan rate of 1 mV/s. The CNT/NF substrate exhibits very low charge storage capability as shown in Fig. 17 (c); The mass loading of the CBD-deposited Ni(OH)<sub>2</sub> on CNT/NF substrates were determined by the weight difference of the total electrode mass before and after the CBD process. This asymmetric supercapacitors exhibited a significantly elevated cell voltage of 1.8 V and a specific capacitance up to 112.5 F g<sup>-1</sup> at a charge/discharge current density of 2.5 mA cm<sup>-2</sup>. The corresponding power density and energy density were 95 Wh kg<sup>-1</sup> and 50.6 W kg<sup>-1</sup>, respectively. At a high charge/discharge current density of 50 mA cm<sup>-2</sup>, its energy density remained at 32.5 Wh kg<sup>-1</sup> and exhibited excellent cycling stability with only 17 % performance lost after

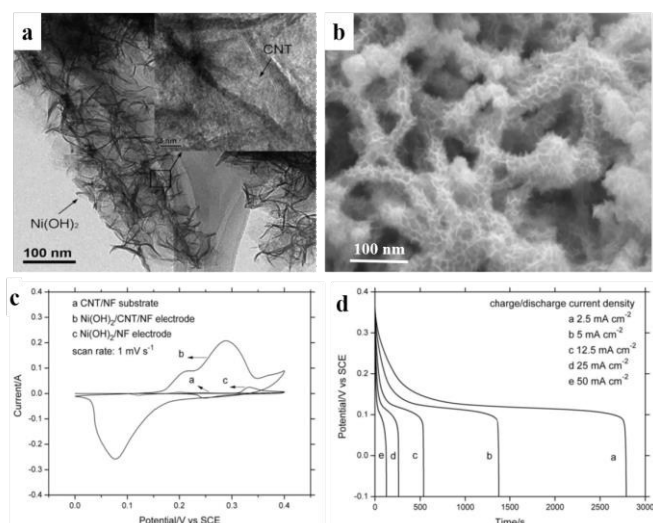


**Fig. 17** (a) TEM image of as-deposited Ni(OH)<sub>2</sub>/CNT composites, inset: enlarged view of Ni(OH)<sub>2</sub>/CNT composite showing graphitic walls of the in situ grown CNTs; (b) SEM images of Ni(OH)<sub>2</sub>/CNT/NF; (c) CV curves of CNT/NF, Ni(OH)<sub>2</sub>/CNT/NF and Ni(OH)<sub>2</sub>/NF electrodes at a scan rate of 1 mV s<sup>-1</sup>; (d) Discharge curves of Ni(OH)<sub>2</sub>/CNT/NF electrode. Adapted with permission from ref. 230, ©2015 The Royal Society of Chemistry.

3000 cycles. The discharge curves of the Ni(OH)<sub>2</sub>/CNT/NF electrode at different charge/discharge currents are shown in Fig. 17 (d). It clearly indicated that Ni(OH)<sub>2</sub>/CNT/NF electrode can provide a more reliable capacitive performance at high rates for high power applications. From the CV results, the specific capacitance and area-normalized capacitance of the Ni(OH)<sub>2</sub>/CNT/NF electrodes, excluding the contribution from the CNT/NF substrate, were calculated to be about 3300 F g<sup>-1</sup> and remarkable synergistic effects provided by the hierarchical 16 F cm<sup>-2</sup> (based on the mass of Ni(OH)<sub>2</sub>). The Ni(OH)<sub>2</sub>/NF electrode without CNT support, prepared by direct Ni(OH)<sub>2</sub> deposition onto NFs exhibited a lower specific capacitance of 2820 F g<sup>-1</sup> and a considerably reduced mass loading ability of 0.25 mg cm<sup>-2</sup>. The ultra-high specific capacitance of the Ni(OH)<sub>2</sub>/CNT/NF electrode was mainly attributed to the well-dispersed Ni(OH)<sub>2</sub> nano-flakes on the high surface area CNT/NF current collector. At different discharge currents, the capacitance lost 33 % of the Ni(OH)<sub>2</sub>/CNT/NF electrode at 10 A g<sup>-1</sup> (50 mA cm<sup>-2</sup>), in contrast to 68 % lost of the Ni(OH)<sub>2</sub>/CNT-based electrode at 12 A g<sup>-1</sup> (6 mA cm<sup>-2</sup>) reported previously.<sup>231</sup>

Alternatively, Xia et al. reported a CNT/Ni(OH)<sub>2</sub>-based supercapacitors, which had a much greater increase in specific capacitance value and excellent cycling ability.<sup>232</sup> The specific capacitance of 50 wt % multi-walled nanotubes (MWNT)-containing Ni(OH)<sub>2</sub> increased from 218 F g<sup>-1</sup> to 310 F g<sup>-1</sup> at a current density of 0.1 A g<sup>-1</sup> and more than 95 % capacity was retained after 2000 cycles. CNTs with large surface area and good conductivity clearly provided good cycling stability of EDLC behavior as well as enhanced capacitance. However, the specific capacitance value became low since a large amount of CNTs was incorporated into Ni(OH)<sub>2</sub> in order to improve the overall capacitor performance. Another possible way to improve the conductivity of poorly conducting Ni(OH)<sub>2</sub> is to incorporate a highly conductive metal with pseudo-capacitor materials.

Dubal et al. used a “bottom-up” approach chemical method to coat nanocrystalline Ni(OH)<sub>2</sub> onto multiwalled carbon nanotubes (MWCNTs) for flexible supercapacitor electrodes, the Ni(OH)<sub>2</sub>/MWCNT films exhibited a specific capacitance of 1487 F g<sup>-1</sup> at a scan rate of 5 mV s<sup>-1</sup>. Ni(OH)<sub>2</sub>/MWCNT demonstrated excellent long-term cyclic stability (96% capacity retention after 1000 cycles).<sup>233</sup>

Using a glucose-assisted hydrothermal method, Dai et al. grew Ni<sub>3</sub>S<sub>2</sub> nano-particles on multi-walled carbon nanotubes, and the materials manifested specific capacitive properties of 1024 F g<sup>-1</sup> at 0.8 A g<sup>-1</sup>, and about 80 % of the initial capacitance could be maintained after 1000 cycles at 3.2 A g<sup>-1</sup>.<sup>234</sup> Zhu et al. synthesized Ni<sub>3</sub>S<sub>2</sub> nanosheets on carbon nanotubes by an efficient multi-step transformation route and the electrode exhibited a maximum specific capacitance of 514 F g<sup>-1</sup> at a current density of 4 A g<sup>-1</sup>.<sup>84</sup>

## 7.2 Combined with graphene

Graphene, due to its high conductivity (26 000 S cm<sup>-1</sup>)<sup>235</sup> and high specific surface area (2630 m<sup>2</sup> g<sup>-1</sup>, theoretical value),<sup>236</sup> provides good electron transfer paths and ensures the direct contact of Ni(OH)<sub>2</sub> nanoparticles with graphene, i.e., reliable electrical contact.

### 7.2.1 Ni(OH)<sub>2</sub> combined with reduced graphene oxide

Min et al. designed and synthesized Ni(OH)<sub>2</sub>/RGO/Ni(OH)<sub>2</sub> composite films on Ni foam through a facile hydrothermal process.<sup>231</sup> The lower layer of Ni(OH)<sub>2</sub>, covered with a thin reduced graphene oxide (RGO) film, is transformed in situ from the surface of a Ni foam substrate through the redox reaction of elemental Ni and graphene oxide. The upper layer of Ni(OH)<sub>2</sub> nanoflakes are vertically assembled on the top surface of the RGO at the lower RGO/Ni(OH)<sub>2</sub> layer. Because the two Ni(OH)<sub>2</sub> layers were different in terms of their Ni<sup>2+</sup> source, particle size, morphology, they were like composites from different metal oxides or hydroxides, the structure was regarded as a “pseudo-composite”. This Ni(OH)<sub>2</sub>/RGO pseudocomposite film has a high specific capacitance of 3328.7 F g<sup>-1</sup> (1.5 A g<sup>-1</sup>), an area-normalized capacitance of up to 15.65 F cm<sup>-2</sup> (mass loading of 4.7 mg cm<sup>-2</sup>, current density of 7 mA cm<sup>-2</sup>). In addition, this pseudocomposite can strongly buffer the volume changes from the phase transformation of Ni(OH)<sub>2</sub> during charging and discharging, due to the flexible framework constructed of porous nanosized Ni(OH)<sub>2</sub>, soft and high strength graphene, and uneven bottom Ni(OH)<sub>2</sub> layer with high adhesion to the NFs substrate. Therefore, this pseudocomposite features excellent cycling stability up to 5000 cycles (90.6 % capacity retention, at 20 mA cm<sup>-2</sup>).

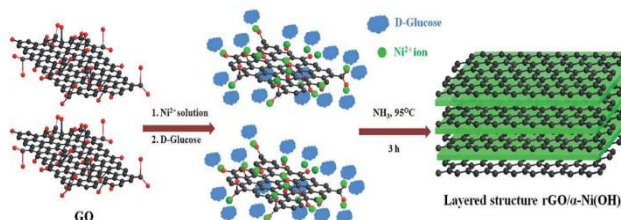


**Fig. 18** Illustrating the growth of layered RGO/α-Ni(OH)<sub>2</sub> hybrid material. Adapted with permission from ref. 237, ©2015 The Royal Society of Chemistry.

Bag et al. synthesized a novel layered hybrid material by a facile one-step strategy, which is shown in Fig. 18.<sup>237</sup> The hybrid materials showed specific capacitance, 1672, 1660, 1520, 1339 and 1250  $F g^{-1}$  at the current density of 1, 2, 4, 10, and 20  $A g^{-1}$ , respectively. Although some capacitance loss was noticed while increasing the current density, the performance of the hybrid materials were superior to the physical mixture and the free  $\alpha-Ni(OH)_2$ . It also retained 81% of the initial capacitance after 2000 cycles. The high electronic conductivity and large surface area of the hybrid materials favor a facile charge transport, the layer structure enhances the overall performance and ensures the easy diffusion of electrolytes ions. An asymmetric supercapacitors device was built base on the hybrid materials with RGO, delivered a high energy density of 42.67  $Wh kg^{-1}$  at a power density of 0.4  $kW kg^{-1}$ .

Yan et al. reported a graphene/ $Ni(OH)_2$ -based supercapacitors that presents increased specific capacitance and relatively good rate capability.<sup>65</sup> The specific capacitance of 21 wt % graphene-containing  $Ni(OH)_2$  increased from  $\sim 1600 F g^{-1}$  to  $1735 F g^{-1}$  at a scan rate of  $1 mV s^{-1}$  and more than 30 % capacitance was retained at a high scan rate of  $50 mV s^{-1}$ . Graphene with good conductivity provided the facile channels for fast electron transfer while  $Ni(OH)_2$  with Faradic behavior offered high specific capacitance. Coupling of graphene in order to improve the conductivity and stability of  $Ni(OH)_2$  were meaningful since it was cost-efficient and effective. However, the rate capability was still low and the fabrication process for graphene with good performance was complicated and tedious.

### 7.2.2 Three dimensional Ni foam-supported graphene oxide

Zheng et al. firstly demonstrated a cheap yet effective method to fabricate three dimensional Ni foam-supported graphene oxide (3D-NiGO).<sup>238</sup> In this case, GO was directly deposited on 3D commercially Ni foam, the GO possessed hydrophobic polyaromatic islands of unoxidized benzene rings and hydrophilic carboxylic acid, epoxy, hydroxyl. The SEM image of as-prepared 3D-NiGO is shown in Fig. 19 (c), it can be directly used as supercapacitors electrode without other current collectors and binders, simplifying the process and decreasing the production cost. Benefiting from the above-mentioned synergistic effects, the 3D-NiGO electrodes showed excellent rate capability, high specific capacity and good cycling stability. The impressive capacitance of  $236 F g^{-1}$  at a current density of  $0.5 A g^{-1}$  was achieved, higher than 3D-NiG ( $148 F g^{-1}$ ), GO ( $78 F g^{-1}$ ) and those reported previously for graphene or GO-based hybrids.

### 7.2.3 $NiCo_2O_4$ grown on graphene-nickel foam

Yu et al. investigated 1D NCO on 3D graphene foam directly as electrode.<sup>239</sup> The NCO nanoneedles were grown vertically on graphene-nickel foam (GNF) by a two-step approach. Firstly, the graphene coated on nickel foam was prepared based on the modified Chen's method.<sup>240</sup> Pure graphene foam cracked easily, so GNF was used as mechanical skeleton. Then, NCO nanoneedles were grown on GNF via hydrothermal treatment and following calcination. The SEM image of the as-prepared NCO nanoneedles on GNF is shown in Fig. 19 (e). The GNF was employed as the current collector without binder and conducting agent, which reduced the connection resistance between the current collector and active material. The NCO nanoneedles exhibited remarkable performance

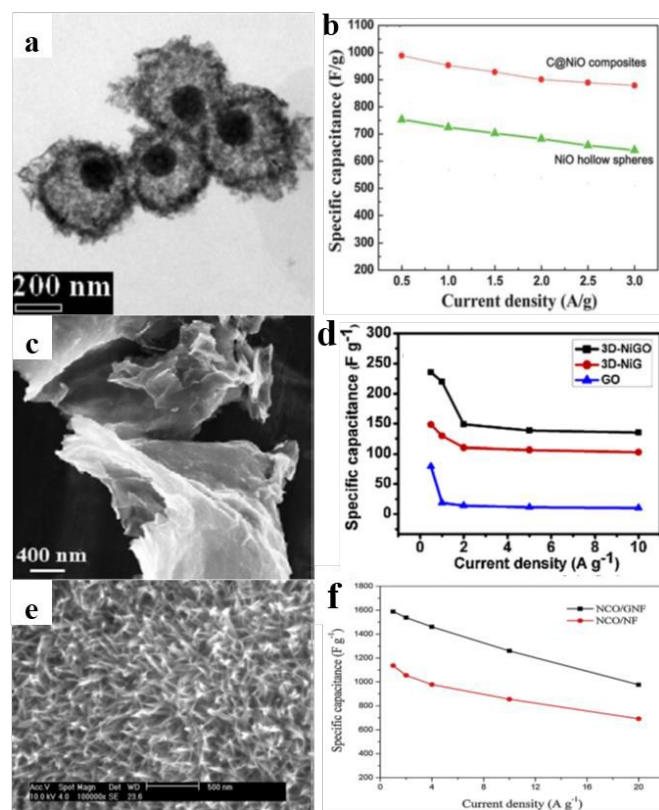


**Fig. 19** SEM images of (a) C@NiO composites, (c) 3D-NiGO, (e) NCO nanoneedles on GNF; Specific capacitance as a function of currents for (b) C@NiO composites and NiO hollow spheres; (d) 3D-NiGO; (f) Specific NCO/GNF and NCO/NF electrodes; (a, b) Adapted with permission from ref. 153; (c, d) ref. 238; (e, f) ref. 239, © 2014 Elsevier; © 2012 The Royal Society of Chemistry.

in supercapacitors, the specific capacitance of NCO nanoneedles were 1588, 1537.6, 1460.8, 1260 and  $976 F g^{-1}$  at 1, 2, 4, 10 and 20  $A g^{-1}$  respectively, 61.46 % of the capacitance was maintained when the current density changed from  $1 A g^{-1}$  to  $20 A g^{-1}$ . As a contrast, the specific capacitance of NCO nanoneedles on NFs were 1136.2, 1055.2, 978.4, 856 and  $692 F g^{-1}$  at 1, 2, 4, 10 and 20  $A g^{-1}$  respectively, the capacitance retention was 60.9 % at  $20 A g^{-1}$ , which were smaller than that of NCO/GNF.

### 7.2.4 Nickel sulfide combined with graphene

Recently, Zhang et al. successfully synthesized porous  $Ni_3S_2$ -RGO composites directly on NFs using *Bacillus subtilis* as spacers. This electrode showed a relatively high specific capacitance of  $1424 F g^{-1}$  at  $0.75 A g^{-1}$ . However, the mass loading of these electrodes were relatively low, which limited their practical application. And the specific capacitance were unsatisfactory even at the low mass loading because the specific capacitance was much lower than its theoretical value of  $2412 F g^{-1}$ .<sup>241</sup>

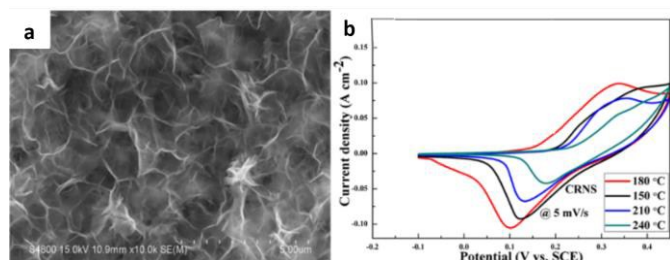


**Fig. 20** FESEM images of (a) CRNS-180 composite, cyclic voltammograms of (b) CRNS-150, 180, 210, and 240 at  $5 \text{ mV s}^{-1}$ ; inset, cyclic voltammograms of contrast samples at  $5 \text{ mV s}^{-1}$ . Adapted with permission from ref. 242, © 2015 American Chemical Society.

Zhang et al. combined  $\text{Co}_9\text{S}_8$ ,  $\text{Ni}_3\text{S}_2$ , and RGO to construct graphene composites with two mixed metal sulfides components.<sup>242</sup> The composites of  $\text{Ni}_3\text{S}_2$ ,  $\text{Co}_9\text{S}_8$ , and RGO were synthesized through a one-step hydrothermal process, they were hydrothermal-assisted synthesized on NFs, NFs acted as both substrate and Ni source for composite films. Fig. 20 (a) shows the FESEM image of  $\text{Co}_9\text{S}_8/\text{RGO}/\text{Ni}_3\text{S}_2$  (CRNS)-180 composites, Fig. 20 (b) shows the results of cyclic voltammograms of CRNS-150, 180, 210, and 240 at  $5 \text{ mV s}^{-1}$ . Charge-discharge measurements were  $80 \text{ mA cm}^{-2}$  (corresponding to 13.53, 12.29, 11.59, 10.73, 10.41, 10.03, and  $9.40 \text{ F cm}^{-2}$ ), respectively. It was found that the  $\text{Co}_9\text{S}_8/\text{RGO}/\text{Ni}_3\text{S}_2/\text{NF}$  electrode exhibited superior capacitive performance with high capability ( $13.53 \text{ F cm}^{-2}$  at  $20 \text{ mA cm}^{-2}$ , i.e.,  $2611.9 \text{ F g}^{-1}$  at  $3.9 \text{ A g}^{-1}$ ), compared with the  $\text{Co}_9\text{S}_8/\text{Ni}_3\text{S}_2$  (CNS) electrode ( $7.02 \text{ F cm}^{-2}$  at  $20 \text{ mA cm}^{-2}$ ) and the  $\text{RGO}/\text{Ni}_3\text{S}_2$  (RNS) electrode ( $7.77 \text{ F cm}^{-2}$  at  $20 \text{ mA cm}^{-2}$ ) prepared under identical conditions. When the current density increased from  $3.9$  to  $15.6 \text{ A g}^{-1}$ ,  $69.5 \%$  capacitance were retained ( $1814.7 \text{ F g}^{-1}$  vs  $2611.9 \text{ F g}^{-1}$ ), suggesting excellent rate capability and enhanced electrochemical stability, with  $91.7 \%$  remained after 1000 continuous charge-discharge cycles even at a high current density of  $80 \text{ mA cm}^{-2}$ .

Li et al. demonstrated a facile and scalable process to fabricate  $\text{MCs@GNS@NiS}$  electrode through “dip and dry” and electrodeposition methods.<sup>243</sup> A piece of macroporous commercially available make-up cottons (MCs), made of randomly intertwined polyester fibers, was cleaned by acetone and DI water for several times, following by completely dried at  $100 \text{ }^\circ\text{C}$  for 24 h. Then, the MCs were dipped into the graphene oxide solution ( $3 \text{ mg mL}^{-1}$ ) prepared by the modified Hummer's method. Due to strong absorption, the GO quickly coated the MCs (denoted as  $\text{MCs@GO}$ ). The “wet” MCs were placed in a vacuum oven ( $100 \text{ }^\circ\text{C}$ ) for 10 min to remove water. This simple “dip and dry” process was repeated for a number of times to increase the GO loading. After 25 cycles of dipping and drying, the MCs were dipped into hydroiodic acid and heated up to  $85 \text{ }^\circ\text{C}$  for 1 min, then washed with a large amount of DI water and ethanol. Finally, the MCs were dried in vacuum oven at  $100 \text{ }^\circ\text{C}$  for 24 h. The porous NiS thin films on  $\text{MCs@GNS}$  (graphene nanosheets) were electrodeposited in a three-electrode system, while Pt sheet and  $\text{Ag}/\text{AgCl}$  electrode served as the auxiliary electrode and the reference electrode, respectively. The electrodeposition solution was composed of nickel chloride hexahydrate ( $0.1 \text{ M}$ ) and thiourea ( $1 \text{ M}$ ). The electrodeposition voltage was set as  $0.9 \text{ V}$  and lasted for several minutes at room

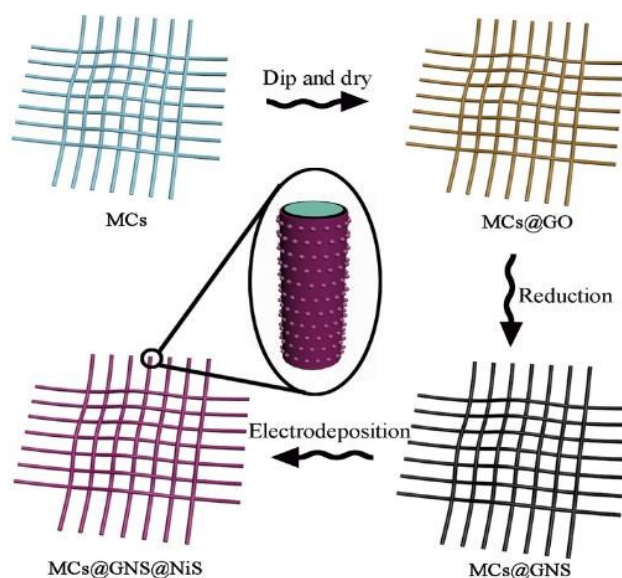


**Fig. 21** The schematic illustration of the preparation of  $\text{MCs@GNS@NiS}$  composite. Adapted with permission from ref. 243, © 2014 Elsevier.

temperature using an electrochemical workstation (VMP3/Z Bio-Logic). After the electrodeposition, the MCs were taken out and carefully washed with DI water to remove excessive electrolyte, and then placed in vacuum oven at  $40 \text{ }^\circ\text{C}$  for 24 h. The processes of the preparation are briefly described by Fig. 21.

The 3D microporous MCs coated with GNS served as excellent conductive networks for fast transmission of electrons and electrolytes to active electrode materials. The porous NiS films with rough surface, which tightly covered on the surface of  $\text{MCs@GNS}$  composites, provided a high electrode/electrolyte contact area and short ions diffusion path. Based on the above characteristics, the specific capacitances of  $\text{MCs@GNS@NiS}$  electrode were as high as 775, 715, 632, 570,  $503 \text{ F g}^{-1}$  at current densities of 0.5, 1, 2, 3,  $5 \text{ A g}^{-1}$ , it also exhibited good capacitive retention of  $88.1 \%$  after 1000 cycles at  $2 \text{ A g}^{-1}$ , the columbic efficiency consistently remained above  $92 \%$  within 1000 cycles. The fine specific capacitance and good cycling stability demonstrate that the  $\text{MCs@GNS@NiS}$  electrode has potential for application in supercapacitors.

### 7.2.5 Nickel phosphides combined with graphene

$\text{Ni}_2\text{P}$  nanoparticles grown on RGO were successfully synthesized via the low-temperature solid state reaction method by An et al., they employed  $\text{NiS}_2$  as the precursor and sodium monophosphate as the phosphorus source.<sup>244</sup> The composites were investigated as electrochemical pseudo-capacitor materials for potential energy storage applications. The average specific capacitance of the  $\text{Ni}_2\text{P}/\text{RGO}$  was calculated to be 2984.2, 1835.4, 1365.7, 778.9 and  $453 \text{ F g}^{-1}$  at scan rates of 1, 5, 10, 20 and  $50 \text{ mV s}^{-1}$ , respectively. The discharge specific capacitance loss after 2500 cycles was negligible, indicating the stable cycling performance and high specific capacitance of the  $\text{Ni}_2\text{P}/\text{RGO}$  electrode.

### 7.3 Combined with carbon fibers

Ko et al. synthesized  $(\text{Ni}/\text{Co})\text{O}_x$ -carbon fibers on Ni foam by thermal decomposition of metal salt solutions in the presence of carbon fibers.<sup>245</sup> The specific capacitances of the  $(\text{Ni}/\text{Co})\text{O}_x$  and  $(\text{Ni}/\text{Co})\text{O}_x$ -carbon fiber composite were 936 and  $1271 \text{ F g}^{-1}$  at a scan rate of  $5 \text{ mV s}^{-1}$ , and 612 and  $955 \text{ F g}^{-1}$  when the scan rate was increased to  $100 \text{ mV s}^{-1}$ . The mass loading of the  $(\text{Ni}/\text{Co})\text{O}_x$ -carbon fiber

composite increased from 0.81 to 3.2 6 mg cm<sup>-2</sup>, while providing a high areal capacitance of ~4 F cm<sup>-2</sup>.

## 8. Nickel based metal-organic frameworks

Till now, conventional electrode materials were restricted in application based on the rapid development of supercapacitors with higher performance. Therefore, rapid development of new electrode materials with high performance for supercapacitors is essential.

Metal-organic frameworks (MOFs) or porous coordination polymers (PCPs) were developed around 26 years ago.<sup>246,247</sup> Emerging as a new class of porous materials, MOFs have attracted tremendous attention in recent years mainly because of their designable framework structures, transition-metal clusters as nodes and organic ligands as struts.<sup>248-250</sup>

They have infinite crystalline lattices which generally involve two main components of inorganic vertices and organic struts. The two main components are connected with each other by coordination bonds, together with intermolecular interactions, affording a network that has definite topology with pores. Porous MOFs generally have micro-porous (~2 nm) characters, the pore sizes could be tuned from several angstroms to several nanometers.<sup>251-254</sup> The extensive modulations of pore sizes and framework structures endow MOFs with extraordinary high surface area of 43000 m<sup>2</sup> g<sup>-1</sup>, and the latest Lagmiur surface area record of over 10 000 m<sup>2</sup> g<sup>-1</sup>.<sup>255</sup> These unique characteristics of MOFs set them apart from other traditional porous materials.

### 8.1 Nickel based metal-organic frameworks

MOFs have been successfully used as electrode materials for fuel cells and rechargeable batteries,<sup>256</sup> the introduction of MOFs in supercapacitors has been reported only recently<sup>257,258</sup> and can be classified into two cases. In one case, MOFs are utilized as novel templates for preparing porous carbons<sup>258,260</sup> or metal oxides<sup>261-263</sup>. In the other case, the MOFs can be directly used as a new type of electrode material. Studies on the direct use of MOFs as electrodes are rarer and more challenging due to the structural flexibility of MOFs.<sup>264</sup>

MOFs including Co-,<sup>265,266</sup> Zr-,<sup>267</sup> Fe-,<sup>268</sup> Co-Zn-,<sup>269</sup> In-<sup>270</sup> Zn- and Cd-based materials<sup>271</sup> have been investigated, but only the Co-based MOFs exhibited a capacitance of approximately 200 F g<sup>-1</sup> in LiOH solution.<sup>265</sup> These materials may be considered of limited success due to their poor electrical conductivity and steric hindrance to ion insertion, which influenced the pore size<sup>272,273</sup> and compatibility between these MOFs and the electrolyte.<sup>264</sup> With Ni(Cl)<sub>2</sub>·6H<sub>2</sub>O and 1,3,5-benzenetricarboxylic acid (H<sub>3</sub>btc) as raw materials, Kang et al. successfully synthesized a simple nickel based MOF by a hydrothermal reaction, formulated Ni<sub>3</sub>(btc)<sub>2</sub>·12H<sub>2</sub>O with a structure composed of zigzag chains with both the bridging and terminal Ni<sup>2+</sup> ions, each nickel center coordinated to four water molecules. Ni(Cl)<sub>2</sub>·6H<sub>2</sub>O and 1,3,5-benzenetricarboxylic acid (H<sub>3</sub>btc) had been employed for the first time to synthesize Ni-based MOFs materials. In addition, a simple asymmetric supercapacitor with a high energy density of 16.5 Wh kg<sup>-1</sup> was successfully built using the nickel based MOFs as positive electrode and commercial activated carbon as negative electrode in KOH electrolyte.<sup>274</sup> The test results showed this nickel based MOFs have good pseudo-capacitive

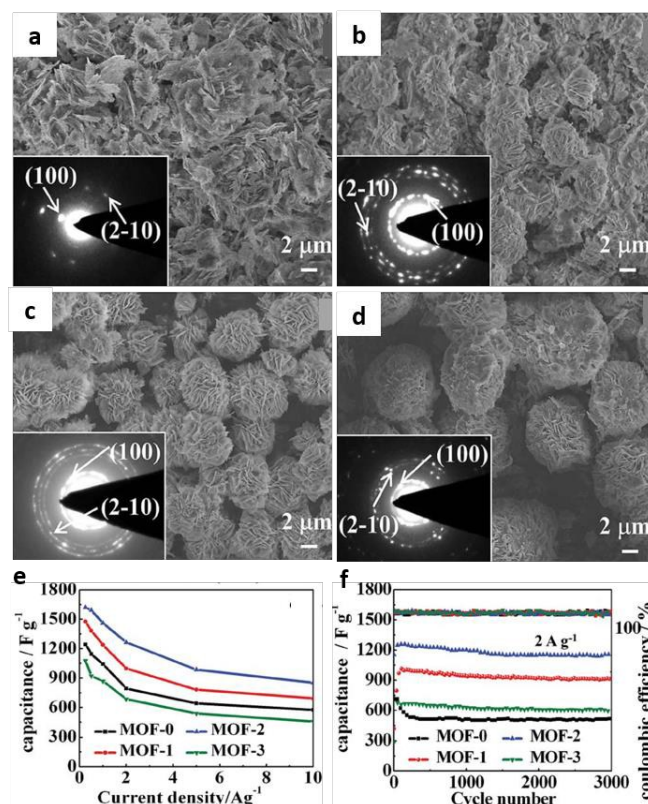


**Fig. 22** SEM images of Zn-doped Ni-MOF materials: (a) MOF-0; (b) MOF-1; (c) MOF-2; (d) MOF-3 (insets: the corresponding SAED patterns); (e) specific capacitances at different current densities, and (f) GCD cycling performance. Adapted with permission from ref. 276, © 2014 The Royal Society of Chemistry.

behavior in KOH aqueous electrolyte, a specific capacitance of 726 F g<sup>-1</sup> was obtained, and it exhibited superior cyclical stability with 94.6% of the initial capacitance over consecutive 1000 cycles.

Wei et al. successfully synthesized a layered two-dimensional (2D) Ni-based MOF and firstly used it as a supercapacitors electrode in an aqueous alkaline solution.<sup>275</sup> This material exhibited large capacitance of 1127 and 668 F g<sup>-1</sup> at rates of 0.5 and 10 A g<sup>-1</sup>, respectively. At the same time, over 90% performance was retained after 3000 cycles. However, the maximum capacitance of 1127 F g<sup>-1</sup> was not remarkable enough for pseudocapacitive materials. To further improving the capacitance, they synthesized a layered structural Zn-doped Ni-MOF, Zn-doped Ni-based MOF materials prepared with different amount of ZnCl<sub>2</sub> (0, 0.0228, 0.0456 and 0.0912 g) denoted as MOF-0, MOF-1, MOF-2 and MOF-3, respectively.<sup>276</sup> The SEM images and electrochemical performance are shown in Fig. 22. These microspheres were firstly used as an electrode material for supercapacitors and exhibited high specific capacitance, good rate capability and good cycling stability. For the capacitances of 1620, 860 F g<sup>-1</sup> were achieved at 0.25, 10 A g<sup>-1</sup>, respectively, and the capacitance lost only 8 % after 3000 cycles.

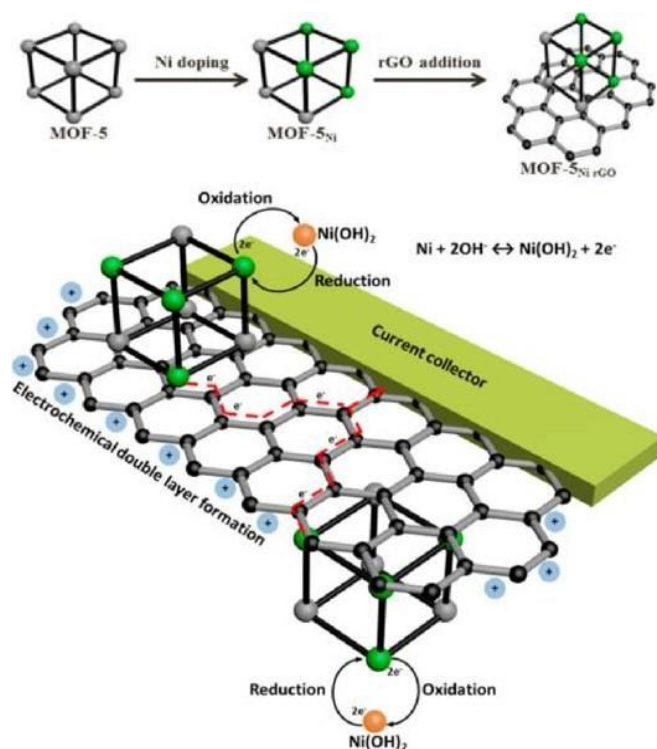


**Fig. 23** Concept for Ni doping and incorporating RGO to form a composite of RGO and Ni-doped MOF-5 and its use as an electrode material that harness both the electrochemical double layer performance of RGO and the reversible redox reactions of Ni metal centers with a synergy that facilitates effective and efficient charge transfer processes. Adapted with permission from ref. 280, © 2015 American Chemical Society.

## 8.2 Nickel based metal-organic frameworks combined with carbon materials

As mentioned above, applying nickel based MOFs materials for supercapacitors has constituted an important prospect, however, the composites binding nickel based MOFs and carbon-based species as electrode materials applied in supercapacitors have been rarely investigated and few methods have been reported. MOFs have been considered as an alternative precursor to construct nanoporous carbons, they may broaden the library of nanoporous carbons with novel structures and properties.<sup>277</sup>

Wen et al. developed a solvothermal method to grow Ni-MOF on the CNT surface, then a novel and durable asymmetric supercapacitor was formed, the supercapacitor based on Ni-MOF/CNT and RGO/C<sub>3</sub>N<sub>4</sub> as the positive and negative electrodes.<sup>278</sup> In the designed structure of Ni-MOF/CNT composites, CNTs were applied as a robust backbone, whose surface can be easily modified by carboxyl groups, facilitating the realization of uniform growth of the Ni-MOF on their surface. Excellent conductivity of CNTs can furnish low ionic diffusion resistance. Meanwhile, CNTs can serve as a current collector to shorten the path length of electron collection/transport. The synergistic effects of CNTs and the Ni-MOF can buffer the large volume change of active species in long-term cycling. The electrochemical performance of the supercapacitor was evaluated at an operating voltage of about 1.6V in 6 M KOH aqueous electrolyte, it presented a high energy density of 36.6 W h kg<sup>-1</sup> at a power density of 480 W kg<sup>-1</sup>, and excellent long cycle life

along with only 5% specific capacitance lost after 5000 cycles. Those superior electrochemical performances encouraged much interest in opening up the possibility of MOF-based composites for numerous applications in asymmetric supercapacitors.

Composites of Ni-doped MOF with RGO were synthesized in bulk (gram scale) quantities by Banerjee et al., the concept was shown in Fig. 23. They adapted a fast synthesis method (direct room temperature mixing approach) and produced bulk quantities of MOF, and Ni doping of MOF-5 (MOF-5<sub>Ni</sub>) used the solvothermal method reported by Yang et al.<sup>279</sup>. The efficient charge transfer process was attributed to the synergy effect between the distributed Ni centers in the MOF-5 and interconnected graphene nanosheets. MOF-5 Ni 50% RGO 50% as an energy storage realized energy density of 37.8Wh/kg at a power density of 226.7 W/kg, and exhibited large stability during cycling.<sup>280</sup>

## Conclusions and outlooks

Generally, this review has introduced the producing method, morphology and electrochemical properties of several types of important nickel based materials. We also evaluated recent advances in nickel based materials for high performance pseudo-capacitor electrodes, giving sufficiently good controllability on their structural and textural properties that are significant for surface redox reactions. Nickel compounds have intrinsically low electrical conductivity, doping with conductive oxides or integration with conductive carbon nanomaterials can improve the conductivity and enhance the pseudo-capacitive behaviors of the composite materials. Those composite materials show excellent capacitance values, high rate capabilities and good charge/discharge cycling stabilities.

It is our opinion that several future trends of nickel based materials for high-performance pseudo-capacitors can be noted as follows:

- (1) To further increase the Cs value through controlling the morphology, surface area, particle size and pore properties. Nanostructure of nickel based materials with high specific surface area can make efficient contact with the electrolyte ions, providing more electro-active sites for energy storage, keeping high charge and discharge capacity even under high current density.
- (2) To improve the conductivity by forming composite materials. Composites not only embody the advantages of all constituents but also overcome the drawbacks of individual components. In recent years, novel carbon nanomaterials as well as the various existing forms provide versatile platforms for integrating nickel compounds and their composites. Those novel carbon nanomaterials mainly includes graphene foam, graphene quantum dots, "activated" graphene.<sup>281,282</sup> The synergistic combination of the carbon nanomaterials with nickel oxides can maximize the benefits from all components, making this approach one of the most effective methods to improve the conductivity of nickel based materials.
- (3) To achieve high energy and power density synchronously by constructing asymmetric capacitor. Restricted by the intrinsic electrochemical properties of nickel compounds,

the operating potential window is very small. Combining nickel compounds as positive electrodes and carbon nanomaterials/iron oxides as negative electrodes to form asymmetric capacitors, the obtained capacitors could possibly have a higher potential window which will enhance the energy storage. By designing electrolytes for optimum electrochemical performance in such asymmetric configurations, a high-voltage operation may be achieved without compromising long-term cycling stability. However, critical factors for optimizing the device electrochemical performance remain to be explored, and the search for new nickel based materials with high performance remains an important area in supercapacitors.

However, Brousse et. al proposed that the term "pseudocapacitive" must be only used to describe electrode materials such as  $\text{MnO}_2$  that displays an electrochemical behavior typical of that observed for a capacitive carbon electrode in mild aqueous electrolyte. It's confused that  $\text{Ni}(\text{OH})_2$  or cobalt oxides which are the same term for materials might exhibit high-rate capability, but with the electrochemical signature of a "battery" electrode.<sup>283</sup> There were situations where the electrochemical behavior of a faradaic electrode can appear pseudocapacitive. The electrode material (powder, thin film...) reaches a critical size<sup>284</sup> where diffusion occurs through very limited 5 time scales, giving rise to a "capacitive like" behavior. For  $\text{Ni}(\text{OH})_2$ , there are hundreds of papers dealing with the pseudocapacitive nature of cobalt-based oxides or hydroxides, or even nickel-cobalt oxides or hydroxides, which clearly exhibit a non-linear dependence of the charge stored vs the potential window. There are some studies that point out the faradaic nature of nickel-cobalt oxide electrodes, which are denominated as high-rate capability positive electrodes for asymmetric devices.<sup>285</sup> It is promising that such high-rate capability electrodes are of great interest when coupled with a capacitive carbon negative electrode to design asymmetric (hybrid) devices with improved rate capability.

## Acknowledgements

This work is supported by the Program for New Century Excellent Talents of the University in China (grant no. NCET-13-0645) and National Natural Science Foundation of China (NSFC-21201010, 21173183, 51202106), Plan For Scientific Innovation Talent of Henan Province, Program for Innovative Research Team (in Science and Technology) in University of Henan Province (14IRTSTHN004), the Science & Technology Foundation of Henan Province (122102210253 and 13A150019), and the China Postdoctoral Science Foundation (2012M521115). We also acknowledge the Priority Academic Program Development of Jiangsu Higher Education Institutions and the technical support received at the Testing Center of Yangzhou University.

## Abbreviation Index

Electric double layer capacitors: EDLCs  
Electrochemical capacitors: ECs  
The 17th annual international electric vehicles: EVS-17  
Metal oxides: MOs  
Supercapacitor: SC  
One-dimensional: 1D  
Carbon fiber paper: CFP  
NiO nanoparticles: NPs  
Cyclic voltammetry: CV  
Cyclic chronopotentiometry: CC  
Reduced graphene oxide: RGO  
Graphene oxide: GO  
Chemical vapor deposition: CVD  
Chemical bath deposition: CBD  
Multi-walled nanotube: MWNT  
Carbon nanotubes: CNTs  
Nanowires: NWS  
3-dimensional: 3D  
3DGN: three-dimensional graphene network  
Nickel foams: NFs  
 $\text{NiCo}_2\text{O}_4$ : NCO  
 $\text{Co}_9\text{S}_8/\text{Ni}_3\text{S}_2$ : CNS  
RGO/ $\text{Ni}_3\text{S}_2$ : RNS  
 $\text{Co}_9\text{S}_8/\text{RGO}/\text{Ni}_3\text{S}_2$ : CRNS  
Activated carbon: AC  
 $\text{NiC}_2\text{O}_4$ - nanotubes: NCO-NTs  
Nanowire arrays: NWAs  
Nanosheet arrays: NSAs  
Thioacetamide: TAA  
Three dimensional Ni foam-supported graphene oxide: 3D-NiGO  
Graphene-nickel foam: GNf  
Make-up cottons: MCs  
GNS: graphene nanosheets  
Nanosheet arrays: NSAs  
Nickel/cobalt layered double hydroxides: Ni/Co-LDH  
Layered double hydroxides: LDH  
Nanotube arrays: NTAs

## Notes and references

- 1 X. Dong, Z. Guo, Y. Song, M. Hou, J. Wang, Y. Wang and Y. Xia, *Adv. Funct. Mater.*, 2014, **24**, 3405.
- 2 Y. Wang, D. Zhou, D. Zhao, M. Hou, C. Wang and Y. Xia, *J. Electrochem. Soc.*, 2013, **160**, A98.
- 3 P. Simon, Y. Gogotsi and B. Dunn, *Science*, 2014, **343**, 1210.
- 4 J. Zhang and X. S. Zhao, *ChemSusChem*, 2012, **5**, 818.
- 5 S. Chen, W. Xing, J. Duan, X. Hu and S. Z. Qiao, *J. Mater. Chem. A*, 2013, **1**, 2941.
- 6 K. Naoi, *Fuel Cells*, 2010, **10**, 825.
- 7 K. Lee, W. Chin and C. Sow, *J. Mater. Chem. A*, 2014, **2**, 17212.
- 8 L. Zhang, X. Zhao, *Chem. Soc. Rev.*, 2009, **38**, 2520.
- 9 G. Wang, L. Zhang, J. Zhang, *Chem. Soc. Rev.*, 2012, **41**, 797.

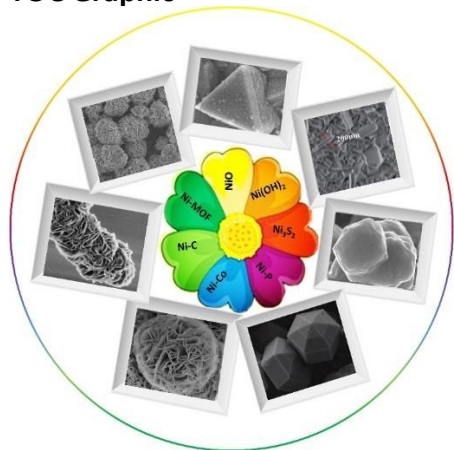
- 10 H. Wang and H. Dai, *Chem. Soc. Rev.*, 2013, **42**, 3088.
- 11 L. H. Bao, J. F. Zang and X. D. Li, *Nano Lett.*, 2011, **11**, 1215.
- 12 S. Biswas and L. T. Drzal, *Chem. Mater.*, 2010, **22**, 5667.
- 13 Y. Wang, Y. Xia, *Adv. Mater.*, 2013, **37**, 5336.
- 14 M. Winter, R. Brodd, *Chem. Rev.*, 2004, **104**, 4245.
- 15 A. Arico, P. Bruce, B. Scrosati, J. Tarascon and W. Schalkwijk, *Nat. Mater.*, 2005, **4**, 366.
- 16 V. Subramanian, H. Zhu, R. Vajtai, P. Ajayan and B. Wei, *J. Phys. Chem. B*, 2005, **109**, 20207.
- 17 L. Yuan, X. Xiao, T. Ding, J. Zhong, X. Zhang, Y. Shen, B. Hu, Y. Huang, J. Zhou and Z. Wang, *Angew. Chem. Int. Ed.*, 2012, **51**, 4934.
- 18 N. Liu, W. Ma, J. Tao, X. Zhang, J. Su, L. Li, C. Yang, Y. Gao, D. Golberg and Y. Bando, *Adv. Mater.*, 2013, **25**, 4925.
- 19 L. Chen, Z. Huang, H. Liang, Q. Guan and S. Yu, *Adv. Mater.*, 2013, **25**, 4746.
- 20 S. Han, D. Wu, S. Li, F. Zhang and X. Feng, *Adv. Mater.*, 2014, **26**, 849.
- 21 P. Simon and Y. Gogotsi, *Nat. Mater.*, 2008, **7**, 845.
- 22 J. Jiang, Y. Li, J. Liu, X. Huang, C. Yuan and X. W. Lou, *Adv. Mater.*, 2012, **24**, 5166.
- 23 W. Wei, X. Cui, W. Chen and D. G. Ivey, *Chem. Soc. Rev.*, 2011, **40**, 1697.
- 24 Y. Wang, Y. Zhao and C. Xu, *J. Solid State Electrochem.*, 2011, **16**, 829.
- 25 Z. Lu, Q. Yang, W. Zhu, Z. Chang, J. Liu, X. Sun, D. Evans and X. Duan, *Nano Res.*, 2012, **5**, 369.
- 26 S. Kim, Y. Kim, J. Park and J. Ko, *Int. J. Electrochem. Sci.*, 2009, **4**, 1489.
- 27 L. D. Feng, Y. F. Zhu, H. Y. Ding, C. Y. Ni, *J. Power Sources*, 2014, **267**, 430.
- 28 H. Pang, Y. Shi, J. Du, Y. Ma, G. Li, J. Chen, J. Zhang, H. Zheng, B. Yuan, *Electrochim. Acta*, 2012, **85**, 256.
- 29 H. Pang, Q. Lu, Y. Li and F. Gao, *Chem. Commun.*, 2009, 7542.
- 30 J. Zhao, M. Zheng, Z. Run, J. Xia, M. Sun, H. Pang, *J. Power Sources*, 2015, **285**, 385.
- 31 M. Kundu, L. Liu, *Mater. Lett.*, 2015, **144**, 114.
- 32 H. Pang, Y. Ma, G. Li, J. Chen, J. Zhang and H. Zheng, *Dalton Trans*, 2012, **41**, 13284.
- 33 Y. Wang and Y. Xia, *Electrochim. Acta*, 2006, **51**, 3223.
- 34 D. Zhao, M. Xu, W. Zhou, J. Zhang and H. Li, *Electrochim. Acta*, 2008, **53**, 2699.
- 35 S. Xiong, C. Yuan, X. Zhang, B. Xi and Y. Qian, *Chem.-Eur. J.*, 2009, **15**, 5320.
- 36 A. Mondal, D. Su, Y. Wang, S. Chen, Q. Liu and G. Wang, *J. Alloys Compd.*, 2014, **582**, 522.
- 37 J. Bae, M. Song, Y. Park, J. Kim, M. Liu and Z. Wang, *Angew. Chem.* 2011, **123**, 1721.
- 38 S. Cheng, L. Yang, Y. Liu, W. Lin, L. Huang, D. Chen, C. Wong and M. Liu, *J. Mater. Chem. A*, 2013, **1**, 7709.
- 39 S. Kim, J. Lee, H. Ahn, H. Song, J. Jang, *ACS Appl. Mater. Interfaces*, 2013, **5**, 1596.
- 40 Y. Zhang, X. Xia, J. Tu, Y. Mai, S. Shi, X. Wang and C. Gu, *J. Power Sources*, 2012, **199**, 413.
- 41 C. Wu, J. Dai, X. Zhang, J. Yang and Y. Xie, *J. Am. Chem. Soc.*, 2009, **131**, 7218.
- 42 Y. Huang, X. Duan, Y. Cui, L. Lauhon, K. Kim and C. Lieber, *Science*, 2001, **294**, 1313.
- 43 S. Jahromi, A. dikumar, B. Goh, Y. Lim, W. Basirun, H. Lim and N. Huang, *RSC Adv.*, 2015, **5**, 14010.
- 44 Q. Lu, Michael W. Lattanzi, Y. Chen, X. Kou, W. Li, X. Fan, Karl M. Unruh, J. Chen, and John Q. Xiao, *Angew. Chem. Int. Ed.*, 2011, **50**, 6847.
- 45 Z. Lu, Z. Chang, J. Liu, and X. Sun, *Nano Res.*, 2011, **4**, 658.
- 46 S. Kim, M. Kim, W. Lee and T. Hyeon, *J. Am. Chem. Soc.*, 2002, **124**, 7642.
- 47 X. Li, F. Cheng, B. Guo and J. Chen, *J. Phys. Chem. B*, 2005, **109**, 14017..
- 48 Y. Yin, R. Rioux, X. Erdonmez, S. Hughes, G. Somorjai and A. Alivisatos, *Science*, 2004, **304**, 711.
- 49 Y. Sun, B. Mayers and Y. Xia, *Adv. Mater.*, 2003, **15**, 7.
- 50 N. Alhebshi, R. Rakhi and H. Alshareef, *J. Mater. Chem. A*, 2013, **1**, 14897.
- 51 A. Inamdar, Y. Kim, S. Pawar, J. Kim, H. Im, and H. Kim, *J. Power Sources*, 2011, **196**, 2393.
- 52 G. Hu, C. Li and H. Gong, *J. Power Sources*, 2010, **195**, 6977.
- 53 J. Lee, T. Ahn, D. Soundararajan, J. Koc and J. Kim, 2011, **47**, 6305.
- 54 C. Liu, and Y. Li, *J. Alloys Compounds*, 2009, **478**, 415.
- 55 C. Hu, J. Chen and K. Chang, *J. Power Sources*, 2013, **221**, 128.
- 56 Devaraj, S. and Munichandraiah, N., *J. Phys. Chem. C.*, 2008, **112**, 4406.
- 57 L. Mao, K. Zhang, H. Chan and J. Wu, *J. Mater. Chem.*, 2012, **22**, 1845.
- 58 K. Liang, X. Tang and W. Hu, *J. Mater. Chem.*, 2012, **22**, 11062.
- 59 J. Li, F. Luo, X. Tian, Y. Lei, H. Yuan and D. Xiao, *J. Power Sources*, 2013, **243**, 721.
- 60 J. Yan, W. Sun, T. Wei, Q. Zhang, Z. Fan and F. Wei, *J. Mater. Chem.*, 2012, **22**, 11494.
- 61 J. W. Lee, J. M. Ko and J. Kim, *J. Phys. Chem. C.*, 2011, **115**, 19445.
- 62 Y. Wang, S. Gai, C. Li, F. He, M. Zhang, Y. Yan and P. Yang, *Electrochim. Acta*, 2013, **90**, 673.
- 63 Y. Yuan, X. Xia, J. Wu, J. Yang, Y. Chen and S. Guo, *Electrochim. Acta*, 2011, **56**, 2627.
- 64 G. Gund, D. Dubal, S. Jambure, S. Shinde and C. Lokhande, *J. Mater. Chem. A*, 2013, **1**, 4793.
- 65 J. Yan, Z. Fan, W. Sun, G. Ning, T. Wei, Q. Zhang, R. Zhang, L. Zhi and F. Wei, *Adv. Funct. Mater.*, 2012, **22**, 2632.
- 66 Z. Lu, Z. Chang, W. Zhu and X. Sun, *Chem. Commun.*, 2011, **47**, 9651.
- 67 G. Wang, L. Zhang and J. Zhang, *Chem. Soc. Rev.*, 2012, **41**, 797.
- 68 H. Li, M. Yu, F. Wang, P. Liu, Y. Liang, J. Xiao, C. Wang, Y. Tong and G. Yang, *Nat. Commun.*, 2013, **45**, 54.
- 69 S. Chen, J. Zhu, H. Zhou and X. Wang, *RSC Adv.*, 2011, **1**, 484.
- 70 L. Li, J. Xu, J. Lei, J. Zhang, F. McLarnon, Z. Wei, N. Li and F. Pan, *J. Mater. Chem. A*, 2015, **3**, 1953.
- 71 S. Kim, P. Thiyagarajan and J. Jang, *Nanoscale*, 2014, **6**, 11646.
- 72 X. Lang, A. Hirata, T. Fujita and M. Chen, *Nat. Nanotechnol.*, 2011, **6**, 232.
- 73 G. Yang, C. Xu, H. Li, *Chem. Commun.*, 2008, **48**, 6537.
- 74 U. M. Patil, K. V. Gurav, V. J. Fulari, C. D. Lokhande and O. S. Joo, *J. Power Sources*, 2009, **188**, 338.
- 75 L. C. Wu, Y. J. Chen, M. L. Mao, Q. H. Li and M. Zhang, *ACS Appl. Mater. Interfaces*, 2014, **6**, 5168.
- 76 B. Hua, X. Qin, A. Asiri, K. Alamry, A. Al-Youbi and X. Sun, *Electrochim. Acta*, 2013, **107**, 339.
- 77 J. Zhao, J. He, M. Sun, M. Qu and H. Pang, *Inorg. Chem. Front.*, 2015, **2**, 129.
- 78 Y. Su, K. Xiao, N. Li, Z. Liu and S. Qiao, *J. Mater. Chem. A*, 2014, **2**, 13845.
- 79 Y. Lei, J. Li, Y. Wang, L. Gu, Y. Chang, H. Yuan and D. Xiao, *ACS Appl. Mater. Interfaces*, 2014, **6**, 1773.
- 80 D. Guo, H. Zhang, X. Yu, M. Zhang, P. Zhang, Q. Li and T. Wang, *J. Mater. Chem. A*, 2013, **1**, 7247.
- 81 M. Gao, Y. Xu, J. Jiang and S. Yu, *Chem. Soc. Rev.* 2013, **42**, 2986.
- 82 B. Qu, Y. Chen, M. Zhang, L. Hu, D. Lei, B. Lu, Q. Li, Y. Wang, L. Chen and T. Wang, *Nanoscale*, 2012, **4**, 7810.
- 83 T. Zhu, B. Xia, L. Zhou and X. Lou, *J. Mater. Chem.*, 2012, **22**, 7851.
- 84 T. Zhu, H. Wu, Y. Wang, R. Xu and X. Lou, *Adv. Energy Mater.*, 2012, **2**, 1497.

- 85 W. Zhao, X. Zhu, H. Bi, H. Cui, S. Sun and F. Huang, *J. Power Sources*, 2013, **242**, 28.
- 86 W. Wang, S. Wang, Y. L. Gao, K. Wang and M. Liu, *Mater. Sci. Eng.*, 2006, **133**, 167.
- 87 A. Ghezelbash, M. Sigman and B. Korgel, *Nano Lett.* 2004, **4**, 537.
- 88 X. Jiang, Y. Xie, J. Lu, L. Zhu, W. He, Y. Qian, *Adv. Mater.*, 2001, **13**, 1278.
- 89 L. Zhang, J. Yu, M. Mo, L. Wu, Q. Li and K. Kong, *J. Am. Chem. Soc.*, 2004, **126**, 8116.
- 90 H. Li, L. Chai, X. Wang, X. Wu, G. Xi, Y. Liu and Y. Qian, *Cryst. Growth Des.*, 2007, **7**, 1918.
- 91 Y. Hu, J. Chen, W. Chen and X. Li, *Adv. Funct. Mater.*, 2004, **14**, 383.
- 92 L. Mi, Q. Ding, W. Chen, L. Zhao, H. Hou, C. Liu, C. Shen and Z. Zheng, *Dalton Trans.*, 2013, **42**, 5724.
- 93 J. Zhu, Y. Li, S. Kang, X. Wei and P. Shen, *J. Mater. Chem. A*, 2014, **2**, 3142.
- 94 S. Chou and J. Lin, *J. Electrochem. Soc.*, 2013, 160, D178.
- 95 W. Zhou, X. Cao, Z. Zeng, W. Shi, Y. Zhu, Q. Yan, H. Liu, J. Wang and H. Zhang, *Energy Environ. Sci.*, 2013, **6**, 2216.
- 96 H. Huo, Y. Zhao and C. Xu, *J. Mater. Chem. A*, 2014, **2**, 15111.
- 97 C. Wei, C. Cheng, J. Zhao, Y. Wang, Y. Cheng, Y. Xu, W. Du, and H. Pang, *Chem. Asian J.*, 2015, **10**, 679.
- 98 K. Liao and Y. Ni, *Mater. Res. Bull.*, 2010, **45**, 205.
- 99 H. Pang, Y. Liu, J. Li, Y. Ma, G. Li, Y. Ai, J. Chen, J. Zhang and H. Zheng, *Nanoscale*, 2013, **5**, 503.
- 100 A. Panneerselvam, M. Malik, M. Afzaal, P. O'Brien and M. Helliwell, *J. Am. Chem. Soc.*, 2008, **130**, 2420.
- 101 R. Che, L. Peng and W. Zhou, *Appl. Phys. Lett.*, 2005, **87**, 173122.
- 102 Y. Ni, K. Liao, J. Hong and X. Wei, *Cryst. Eng. Comm.*, 2009, **11**, 570.
- 103 R. Alcantara, J. Tirado, J. Jumas, L. Monconduit and J. Fourcade, *J. Power Sources*, 2002, **109**, 308.
- 104 A. Alexander and J. Hargreaves, *Chem. Soc. Rev.*, 2010, **39**, 4388.
- 105 S. Carenco, D. Portehault, C. Boissiere, N. Mezailles and C. Sanchez, *Chem. Rev.*, 2013, **113**, 7981.
- 106 J. Xiang, X. Wang, J. Zhong, D. Zhang and J. Tu, *J. Power Sources*, 2011, **196**, 379.
- 107 J. Liu, J. Jiang, C. Cheng, H. Li, J. Zhang, H. Gong and H. Fan, *Adv. Mater.*, 2011, **23**, 2076.
- 108 R. Hameed and K. Khatib, *Int. J. Hydrogen Energy*, 2010, **35**, 2517.
- 109 J. Li, M. Liu, L. Kong, D. Wang, Y. Hu, W. Har and L. Kang, *RSC Adv.*, 2015, **5**, 41721.
- 110 I. Abu and K. Smith, *J. Catal.*, 2006, **241**, 356.
- 111 H. Wang, Y. Shu, M. Zheng and T. Zhang, *Catal. Lett.*, 2008, **124**, 219.
- 112 P. O'Brien, W. Maneeprakorn and M. Malik, *J. Mater. Chem.*, 2010, **20**, 2329.
- 113 S. Brock, E. Muthuswamy and G. L. Savithra, *ACS Nano*, 2011, **5**, 2402.
- 114 A. Wang, M. Qin, J. Guan, L. Wang, H. Guo, X. Li, Y. Wang, R. Prins and Y. Hu, *Angew. Chem., Int. Ed.*, 2008, **47**, 6052.
- 115 Y. Zhao, Y. Zhao, H. Feng, J. Shen, *J. Mater. Chem.*, 2011, **21**, 8137.
- 116 J. Yu, A. Wang, J. Tan, X. Li, J. Bokhovenb, Y. Hua, *J. Mater. Chem.*, 2008, **18**, 3601.
- 117 H. Wu, Y. Gao, H. M. Li, *Cryst. Eng. Comm.*, 2010, **12**, 3607.
- 118 D. Wang, L. Kong, M. Liu, W. Zhang, Y. Luo, L. Kang, *J. Power Sources*, 2015, **274**, 1107.
- 119 Y. Lu, J. Liu, X. Liu, S. Huang, T. Wang, X. Wang, C. Gu, J. Tu and S. Mao, *Cryst. Eng. Comm.*, 2013, **15**, 7071.
- 120 Y. Gao, J. Zhao, Z. Run, G. Zhang and H. Pang, *Dalton Trans.*, 2014, **43**, 17000.
- 121 J. Zhao, H. Pang, J. Deng, Y. Ma, B. Yan, X. Li, S. Li, J. Chen and W. Wang, *Cryst. Eng. Comm.*, 2013, **15**, 5950.
- 122 H. Pang, Z. Yan, Y. Wei, X. Li, J. Li, L. Zhang, J. Chen, J. Zhang and H. Zheng, *Part. Part. Syst. Charact.*, 2013, **30**, 287.
- 123 J. Xiao and S. Yang, *RSC Adv.*, 2011, **1**, 588.
- 124 B. Cui, H. Lin, J. Li, X. Li, J. Yang and J. Tao, *Adv. Funct. Mater.*, 2008, **18**, 1440.
- 125 T. Wei, C. Chen, H. Chien, S. Lu and C. Hu, *Adv. Mater.*, 2010, **22**, 347.
- 126 H. Wang, Z. Hu, Y. Chang, Y. Chen, H. Wu, Z. Zhang and Y. Yang, *J. Mater. Chem.*, 2011, **21**, 10504.
- 127 H. Jiang, J. Ma and C. Li, *Chem. Commun.*, 2012, **48**, 4465.
- 128 H. Tan, X. Rui, W. Shi, H. Xu, Yu, H. Hoster, Q. Yan, *ChemPlusChem*, 2013, **78**, 554.
- 129 J. Liu, Y. Li, X. Huang, G. Li and Z. Li, *Adv. Funct. Mater.*, 2008, **18**, 1448.
- 130 M. Tarasevich and B. Efreimov, *Elsevier*, New York 1982, p.227.
- 131 Q. Wang, B. Liu, X. Wang, S. Ran, L. Wang, D. Chen and G. Shen, *J. Mater. Chem.*, 2012, **22**, 21647.
- 132 M. Liu, L. Kong, C. Lu, X. Li, Y. Luo and L. Kang, *ACS Appl. Mater. Interfaces*, 2012, **4**, 4631.
- 133 M. Liu, L. Kong, C. Lu, X. Li, Y. Luo, L. Kang and X. Li, F. Walsh, *J. Electrochem. Soc.*, 2012, **159**, A1262.
- 134 R. Salunkhe, K. Jang, S. Lee and H. Ahn, *RSC Adv.*, 2012, **2**, 3190.
- 135 G. Zhang, H. Wu, H. Hoster, M. Chan-Park and X. Lou, *Energy Environ. Sci.*, 2012, **5**, 9453.
- 136 J. Chang, J. Sun, C. H. Xu, H. Xu and L. Gao, *Nanoscale*, 2012, **4**, 6786.
- 137 X. Wang, W. Liu, X. Lu and P. Lee, *J. Mater. Chem.*, 2012, **22**, 23114.
- 138 X. Lu, X. Huang, S. Xie, T. Zhai, C. Wang, P. Zhang, M. Yu, W. Li, C. Liang and Y. Tong, *J. Mater. Chem.*, 2012, **22**, 13357.
- 139 C. Yuan, J. Li, L. R. Hou, L. Yang, L. She and X. Zhang, *J. Mater. Chem.*, 2012, **22**, 16084.
- 140 H. Wang, C. Holt, Z. Li, X. Tan, B. Amirkhiz, Z. Xu, B. Olsen, T. Stephenson and D. Mitlin, *Nano Res.*, 2012, **5**, 605.
- 141 C. Yuan, J. Li, L. Hou, X. Zhang, L. Shen, and X. Wen (David) Lou, *Adv. Funct. Mater.*, 2012, **22**, 4592.
- 142 H. Wang and X. Wang, *ACS Appl. Mater. Interfaces.*, 2013, **5**, 6255.
- 143 L. Li, S. Peng, Y. Cheah, P. Teh, J. Wang, G. Wee, Y. Ko, C. Wong, and M. Srinivasan, *Chem. Eur. J.*, 2013, **19**, 5892.
- 144 W. Zhu, Z. Lu, G. Zhang, X. Lei, Z. Chang, J. Liu and X. Sun, *J. Mater. Chem. A*, 2013, **1**, 8327.
- 145 K. Xu, R. Zou, W. Li, Y. Xue, G. Song, Q. Li, X. Liu and J. Hu, *J. Mater. Chem. A*, 2013, **1**, 9107.
- 146 Y. Wang, X. Zhang, C. Guo, Y. Zhao, C. Xu and H. Li, *J. Mater. Chem. A*, 2013, **1**, 13290.
- 147 H. Wu, H. Pang and X. W. (David) Lou, *Energy Environ. Sci.*, 2013, **6**, 3619.
- 148 H. Chen, J. Jiang, L. Zhang, H. Wan, T. Qi, D. Xia, *Nanoscale*, 2013, **5**, 8879.
- 149 J. Xiao, L. Wan, S. Yang, F. Xiao, S. Wang, *Nano Lett.*, 2014, **14**, 831.
- 150 L. Yu, L. Zhang, H. B. Wu, X. Lou, *Angew. Chem. Int. Ed.*, 2014, **53**, 1.
- 151 Y. Li, L. Cao, L. Qiao, M. Zhou, Y. Yang, P. Xiao and Y. Zhang, *J. Mater. Chem. A*, 2014, **2**, 6540.
- 152 G. Zhang and X. Lou, *Adv. Mater.*, 2013, **25**, 976.
- 153 W. Du, Z. Zhu, Y. Wang, J. Liu, W. Yang, X. Qian and H. Pang, *RSC Adv.*, 2014, **4**, 6998.
- 154 H. Chen, J. Jiang, L. Zhang, D. Xia, Y. Zhao, D. Guo, T. Qi and H. Wan, *J. Power Sources*, 2014, **254**, 249.
- 155 J. Pu, F. Cui, S. Chu, T. Wang, E. Sheng and Z. Wang, *ACS Sustainable Chem. Eng.*, 2014, **2**, 809.
- 156 H. Wan, J. Jiang, J. Yu, K. Xu, L. Miao, L. Zhang, H. Chen and Y. Ruan, *Cryst. Eng. Comm.*, 2013, **15**, 7649.
- 157 H. Xia, J. Feng, H. Wang, M. Lai, L. Lu, *J. Power Sources*, 2010, **195**, 4410.

- 158 J. Pu, T. Wang, H. Wang, Y. Tong, C. Lu, W. Kong, Z. Wang, *ChemPlusChem*, 2014, **79**, 577.
- 159 D. Cai, D. Wang, C. Wang, B. Liu, L. Wang, Y. Liu, Q. Li and T. Wang, *Electrochim. Acta*, 2015, **151**, 35.
- 160 L. Shen, Q. Che, H. Li, X. Zhang, *Adv. Funct. Mater.*, 2014, **24**, 2630.
- 161 L. Shen, L. Yu, H. Wu, X. Yu, X. Zhang and X. W. (David) Lou, *Nat. Commun.*, 2015, **6**, 6694.
- 162 Y. Zhu, Z. Wu, M. Jing, X. Yang, W. Song and X. Ji, *J. Power Sources*, 2015, **273**, 584.
- 163 T. Yan, R. Li and Z. Li, *Materials Research Bulletin*, 2014, **51**, 97.
- 164 Y. Gu, Z. Lu, Z. Chang, J. Liu, X. Lei, Y. Li, and X. Sun, *J. Mater. Chem. A*, 2013, **1**, 10655.
- 165 L. Yan, R. Li, Z. Li, J. Liu, F. Fang, G. Wang and Z. Gu, *Electrochim. Acta*, 2013, **95**, 146.
- 166 J. Li, M. Yang, J. Wei and Z. Zhou, *Nanoscale*, 2012, **4**, 4498.
- 167 J. Chen, C. Hus and C. Hu, *J. Power Sources*, 2014, **253**, 205.
- 168 X. Lai, J. Halpert and D. Wang, *Energy Environ. Sci.*, 2012, **5**, 5604.
- 169 J. Nai, Y. Tian, X. Guan and L. Guo, *J. Am. Chem. Soc.*, 2013, **135**, 16082.
- 170 M. Shao, F. Ning, Y. Zhao, J. Zhao, M. Wei, D. Evans and X. Duan, *Chem. Mat.*, 2012, **24**, 1192.
- 171 J. Xu, Y. Dong, J. Cao, B. Guo, W. Wang and Z. Chen, *Electrochim. Acta*, 2013, **114**, 76.
- 172 Y. Tao, R. Li, T. Yang and Z. Li, *Electrochim. Acta*, 2015, **152**, 530.
- 173 L. Fan, L. Tang, H. Gong, Z. Yao and R. Guo, *J. Mater. Chem.*, 2012, **22**, 16376.
- 174 M. Wu, Y. Lin, C. Lin and J. Lee, *J. Mater. Chem.*, 2012, **22**, 2442.
- 175 X. Zhu, H. Dai, J. Hu, L. Ding and L. Jiang, *J. Power Sources*, 2012, **203**, 243.
- 176 M. Zhi, C. C. Xiang, J. T. Li, M. Li and N. Q. Wu, *Nanoscale*, 2013, **5**, 72.
- 177 H. Cheng, Z. Lu, J. Deng, C. Chung, K. Zhang and Y. Li, *Nano Res.*, 2010, **3**, 895.
- 178 B. Qu, L. Hu, Y. Chen, C. Li, Q. Li, Y. Wang, W. Wei, L. Chen and T. Wang, *J. Mater. Chem.*, 2013, **1**, 7023.
- 179 G. Zhang, L. Yu, H. E. Hoster and X. W. (David) Lou, *Nanoscale*, 2013, **5**, 877.
- 180 G. Wang, J. Huang, S. Chen, Y. Gao and D. Cao, *J. Power Sources*, 2011, **196**, 5756.
- 181 J. Shaikh, R. Pawa, R. Devan, Y. Ma, P. Salvi, S. Kolekarc and P. Patil, *Electrochim. Acta*, 2011, **56**, 2127.
- 182 Y. Li, S. Chang, X. Liu, J. Huang, J. Yin, G. Wang and D. Cao, *Electrochim. Acta*, 2012, **85**, 393.
- 183 X. Zhang, W. Shi, J. Zhu, D. Kharistal, W. Zhao, B. Lalia, H. Huang and Q. Yan, *ACS Nano*, 2011, **5**, 2013.
- 184 R. Rakhi, W. Chen, M. Hedhili, D. Cha and H. Alshareef, *ACS Appl. Mater. Interfaces*, 2014, **6**, 4196.
- 185 X. Lu, D. Wu, R. Li, Q. Li, S. Ye, Y. Tong and G. Li, *J. Mater. Chem. A*, 2014, **2**, 4706.
- 186 X. Xia, Z. Zeng, X. Li, Y. Zhang, J. Tu, N.C. Fan, H. Zhang and H. Fan, *Nanoscale*, 2013, **5**, 6040.
- 187 P. Tang, Y. Zhao, Y. Wang, C. Xu, *Nanoscale*, 2013, **5**, 8156.
- 188 W. Li, G. Li, J. Sun, R. Zou, K. Xu, Y. Sun, Z. Chen, J. Yang, J. Hu, *Nanoscale*, 2013, **5**, 2901.
- 189 W. Zhou, D. Kong, X. Jia, C. Ding, C. Cheng, G. Wen, *J. Mater. Chem. A*, 2014, **2**, 6310.
- 190 C. Guan, X. Li, Z. Wang, X. Cao, C. Soci, H. Zhang and H. Fan, *Adv. Mater.*, 2012, **24**, 4186.
- 191 X. Liu, S. Shi, Q. Xiong, L. Li, Y. Zhang, H. Tang, C. Gu, X. Wang and J. Tu, *ACS Appl. Mater. Interfaces*, 2013, **5**, 8790.
- 192 W. Hong, J. Wang, L. Niu, J. Sun, P. Gong and S. Yang, *J. Alloys Compd.*, 2014, **608**, 297.
- 193 J. Li, W. Zhao, F. Huang, A. Manivannan and N. Wu, *Nanoscale*, 2011, **3**, 5103.
- 194 X. Wang, H. Liu, X. Chen, D. Evans and W. Yang, *Electrochim. Acta*, 2012, **78**, 115.
- 195 M. Huang, F. Li, J. Ji, Y. Zhang, X. Zhao and X. Gao, *Cryst. Eng. Comm.*, 2014, **16**, 2878.
- 196 W. Du, S. Wei, K. Zhou, J. Guo, H. Pang and X. Qian, *Mater. Res. Bull.*, 2015, **61**, 333.
- 197 M. Liu, L. Kang, L. Kong, C. Lu, X. Ma, X. Li and Y. Luo, *RSC Adv.*, 2013, **3**, 6472.
- 198 B. Senthilkumar, D. Meyrick, Y. Lee and R. Selvan, *RSC Adv.*, 2013, **3**, 16542.
- 199 M. Liu, L. Kong, C. Lu, X. Ma, X. Li, Y. Luo and L. Kang, *J. Mater. Chem. A*, 2013, **1**, 1380.
- 200 D. Cai, B. Liu, D. Wang, Y. Liu, L. Wang, H. Li, Y. Wang, C. Wang, Q. Li and T. Wang, *Electrochim. Acta*, 2014, **115**, 358.
- 201 B. Senthilkumar, K. Vijaya Sankar, R. Kalai Selvan, M. Danielle and M. Manickam, *RSC Adv.*, 2013, **3**, 352.
- 202 W. Hong, J. Wang, P. Gong, J. Sun, L. Niu, Z. Yang, Z. Wang and S. Yang, *J. Power Sources*, 2014, **270**, 516.
- 203 K. Xu, W. Li, Q. Liu, B. Li, X. Liu, L. An, Z. Chen, R. Zou and J. Hu, *J. Mater. Chem. A*, 2014, **2**, 4795.
- 204 X. Xia, J. Tu, Y. Zhang, X. Wang, C. Gu, X. Zhao and H. Fan, *ACS Nano*, 2012, **6**, 5531.0
- 205 L. Jiang, R. Zou, W. Li, J. Sun, X. Hu, Y. Xue, G. He and J. Hu, *J. Mater. Chem. A*, 2013, **1**, 478.
- 206 T. Lin, C. Dai and K. Hung, *Sci. Rep.* 2014, **4**, 7274.
- 207 X. Sun, G. Wang, H. Sun, F. Lu, M. Yu and J. Lian, *J. Power Sources*, 2013, **238**, 150.
- 208 A. Safavi, S. Kazemi and H. Kazemi, *Electrochim. Acta*, 2011, **56**, 9191.
- 209 J. Chen, K. Huang, S. Liu and X. Hu, *J. Power Sources*, 2009, **186**, 565.
- 210 D. Liu, Z. Yang, P. Wang, F. Li, D. Wang and D. He, *Nanoscale*, 2013, **5**, 1917.
- 211 X. Chen, K. Sun, E. Zhang and N. Zhang, *RSC Adv.*, 2013, **3**, 432.
- 212 M. Wu and J. Wu, *J. Power Sources*, 2013, **240**, 397.
- 213 A. Vu, Y. Qian and A. Stein, *Adv. Energy Mater.*, 2012, **2**, 1056.
- 214 H. Jiang, Y. Xu, T. Wang, P. Zhu, S. Yu, Y. Yu, X. Fu, R. Sun and C. Wong, *Electrochimica Acta*, 2015, **166**, 157.
- 215 W. Zhang, L. Kong, X. Ma, Y. Luo and L. Kang, *J. Alloys Compd.*, 2015, **627**, 313.
- 216 S. Yang, X. Wu, C. Chen, H. Dong, W. Hu and X. Wang, *Chem. Commun.*, 2012, **48**, 2773.
- 217 X. Ma, J. Liu, C. Liang, X. Gong and R. Che, *J. Mater. Chem. A*, 2014, **2**, 12692.
- 218 H. Wang, H. Casalongue, Y. Liang and Dai, *J. Am. Chem. Soc.*, 2010, **132**, 7472.
- 219 Y. Chen, B. Qu, L. Hu, Z. Xu, Q. Li and T. Wang, *Nanoscale*, 2013, **5**, 9812.
- 220 H. Jiang, C. Li, T. Sun and J. Ma, *Chem. Commun.*, 2012, **48**, 2606.
- 221 L. Zhang, Z. Xiong and X. Zhao, *J. Power Sources*, 2013, **222**, 326.
- 222 Z. Fan, J. Yan, T. Wei, L. Zhi, G. Ning, T. Li and F. Wei, *Adv. Funct. Mater.*, 2011, **21**, 2366.
- 223 R. Sharma, A. Rastogi and S. Desu, *Electrochim. Acta*, 2008, **53**, 7690.
- 224 L. Huang and T. Wen, A. Gopalan, *Electrochim. Acta*, 2006, **51**, 3469.
- 225 D. Dreyer, S. Park, C. Bielawski and R. Ruoff, *Chem. Soc. Rev.*, 2010, **39**, 228.
- 226 L. Gu, Y. Wang, R. Lu, W. Wang, X. Peng, J. Sha, *J. Power Sources*, 2015, **273**, 479.
- 227 K. He, Q. Wu, X. Zhang and X. Wang, *J. Electrochem. Soc.*, 2006, **153**, A1568.
- 228 Z. Fan, J. Chen, K. Cui, F. Sun, Y. Xu and Y. Kuang, *Electrochim. Acta*, 2007, **52**, 2959.
- 229 X. Ma, Y. Li, Z. Wen, F. Gao, C. Liang, and R. Che, *ACS Appl. Mater. Interfaces*, 2015, **7**, 974.
- 230 Z. Tang, C. Tang and H. Gong, *Adv. Funct. Mater.*, 2012, **22**, 1272.

- 231 S. Min, C. Zhao, Z. Zhang, G. Chen, X. Qian and Z. Guo, *J. Mater. Chem. A*, 2015, **3**, 3641.
- 232 Y. Wang, L. Yu and Y. Xia, *J. Electrochem. Soc.*, 2006, **153**, A743.
- 233 D. Dubal, G. Gund, C. Lokhande and R. Holze, *ACS Appl. Mater. Interfaces*, 2013, **5**, 2446.
- 234 C. Dai, P. Chien, J. Lin, S. Chou, W. Wu, P. Li, K. Wu and T. Lin, *ACS Appl. Mater. Interfaces*, 2013, **5**, 12168.
- 235 C. Park, F. Giustino, C. Spataru, M. Cohen and S. Louie, *Nano Lett.*, 2009, **9**, 4234.
- 236 M. Stoller, S. Park, Y. Zhu and J. An, R. Ruoff, *Nano Lett.*, 2008, **8**, 3498.
- 237 S. Bag and C. Retna Raj, *J. Mater. Chem. A*, 2014, **2**, 17848.
- 238 C. Zheng, J. Zhang, Q. Zhang, B. You and G. Chen, *Electrochim. Acta*, 2015, **152**, 216.
- 239 M. Yu, J. Chen, J. Liu, S. Li, Y. Ma, J. Zhang and J. An, *Electrochim. Acta*, 2015, **151**, 99.
- 240 Z. Chen, W. Ren, L. Gao, B. Liu, S. Pei and H. Cheng, *Nat. Mater.*, 2011, **10**, 424.
- 241 H. Zhang, X. Yu, D. Guo, B. Qu, M. Zhang, Q. Li and T. Wang, *ACS Appl. Mater. Interfaces*, 2013, **5**, 7335.
- 242 Z. Zhang, Q. Wang, C. Zhao, S. Min and X. Qian, *ACS Appl. Mater. Interfaces*, 2015, **7**, 4861.
- 243 Y. Li, K. Ye, K. Cheng, J. Yin, D. Cao, G. Wang, *J. Power Sources*, 2015, **274**, 943.
- 244 C. An, Y. Wang, Y. Wang, G. Liu, L. Li, F. Qiu, Y. Xu, L. Jiao and H. Yuan, *RSC Adv.*, 2013, **3**, 4628.
- 245 Y. Yoon and J. Ko, *Int. J. Electrochem. Sci.*, 2008, **3**, 1340.
- 246 B. Hoskins and R. Robson, *J. Am. Chem. Soc.*, 1989, **111**, 5962.
- 247 B. Hoskins and R. Robson, *J. Am. Chem. Soc.*, 1990, **112**, 1546.
- 248 M. O'Keeffe and O. Yaghi, *Chem. Rev.*, 2012, **112**, 675.
- 249 L. Wang, X. Feng, L. Ren, Q. Piao, J. Zhong, Y. Wang, H. Li, Y. Chen and B. Wang, *J. Am. Chem. Soc.*, 2015, **137**, 4920.
- 250 J. Long and O. Yaghi, *Chem. Soc. Rev.*, 2009, **38**, 1213.
- 251 W. Zhuang, S. Ma, X. Wang, D. Yuan, J. Li, D. Zhao and H. Zhou, *Chem. Commun.*, 2010, **46**, 5223.
- 252 O. Farha, C. D. Malliakas, M. Kanatzidis and J. Hupp, *J. Am. Chem. Soc.*, 2010, **132**, 950.
- 253 H. Jiang, Y. Tastu, Z. Lu and Q. Xu, *J. Am. Chem. Soc.*, 2010, **132**, 5586.
- 254 M. Eddaoudi, J. Kim, N. Rosi, D. Vodak, J. Wachter, M. O'Keeffe and O. Yaghi, *Science*, 2002, **295**, 469.
- 255 H. Furukawa, N. Ko, Y. Go, N. Aratani, S. Choi, E. Choi, A. Yazaydin, R. Snurr, M. O'Keeffe, J. Kim and O. Yaghi, *Science*, 2010, **329**, 424.
- 256 Y. Kobayashi, B. Jacobs, M. Allendorf and J. Long, *Chem. Mater.*, 2010, **22**, 4120.
- 257 A. Almasoudi and R. Mokaya, *J. Mater. Chem.*, 2012, **22**, 146.
- 258 H. Shi, B. Deng, S. Zhong, L. Wang and A. Xu, *J. Mater. Chem.*, 2011, **21**, 12309.
- 259 H. Jiang, B. Liu, Y. Lan, K. Kuratani, T. Akita, H. Shioyama, F. Zong and Q. Xu, *J. Am. Chem. Soc.*, 2011, **133**, 11854.
- 260 A. Amali, J. Sun and Q. Xu, *Chem. Commun.*, 2014, **50**, 1519.
- 261 C. Su, A. Goforth, M. Smith, P. J. Pellechia and H. Loye, *J. Am. Chem. Soc.*, 2004, **126**, 3576.
- 262 F. Meng, Z. Fang, Z. Li, W. Xu, M. Wang, Y. Liu, J. Zhang, W. Wang, D. Zhao and X. Guo, *J. Mater. Chem. A*, 2013, **1**, 7235.
- 263 X. Liu, *Angew. Chem., Int. Ed.*, 2009, **48**, 3018.
- 264 A. Morozan and F. Jaouen, *Energy Environ. Sci.*, 2012, **5**, 9269.
- 265 D. Lee, S. Yoon, N. Shrestha, S. Lee, H. Ahn and S. Han, *Microporous Mesoporous Mater.*, 2012, **153**, 163.
- 266 D. Lee, D. Shinde, E. Kim, W. Lee, I. Oh, N. Shrestha, J. Lee and S. Han, *Microporous Mesoporous Mater.*, 2013, **171**, 53.
- 267 K. Choi, H. Jeong, J. Park, Y. Zhang, J. Kang and O. Yaghi, *ACS Nano*, 2014, **8**, 7451.
- 268 N. Campagnol, R. Romero-Vara, W. Deleu, L. Stappers, K. Binnemans, D. De Vos and J. Fransaer, *ChemElectroChem*, 2014, **1**, 1182.
- 269 R. Diaz, M. Gisela Orcajo, J. A. Botas, G. Calleja and J. Palma, *Mater. Lett.*, 2012, **68**, 126.
- 270 M. Du, M. Chen, X. Yang, J. Wen, X. Wang, S. Fang and C. Liu, *J. Mater. Chem. A*, 2014, **2**, 9828.
- 271 Y. Gong, J. Li, P. Jiang, Q. Li and J. Lin, *Dalton Trans.*, 2013, **42**, 1603.
- 272 A. Fateeva, P. Horcajada, T. Devic, C. Serre, J. Marrot, J. Grenèche, M. Morcrette, J. Tarascon, G. Maurin and G. Ferey, *Eur. J. Inorg. Chem.*, 2010, **24**, 3789.
- 273 G. Combarieu, M. Morcrette, F. Millange, N. Guillou, J. Cabana, C. Grey, I. Margiolaki, G. Ferey and J. M. Tarascon, *Chem. Mater.*, 2009, **21**, 1602.
- 274 L. Kang, S. Sun, L. Kong, J. Lang and Y. Luo, *Chin. Chem. Lett.*, 2014, **25**, 957.
- 275 J. Yang, P. Xiong, C. Zheng, H. Qiu and M. Wei, *J. Mater. Chem. A*, 2014, **2**, 16640.
- 276 J. Yang, C. Zheng, P. Xiong, Y. Li and M. Wei, *J. Mater. Chem. A*, 2014, **2**, 19005.
- 277 W. Chaikittisilp, K. Ariga and Y. Yamauchi, *J. Mater. Chem. A*, 2013, **1**, 14.
- 278 P. Wen, P. Gong, J. Sun, J. Wang and S. Yang, *J. Mater. Chem. A*, 2015, **3**, 13874.
- 279 J. Yang, Q. Liu and W. Sun, *Microporous Mesoporous Mater.*, 2014, **190**, 26.
- 280 P. Banerjee, D. Lobo, R. Middag, W. Ng, M. Shaibani, and M. Majumder, *ACS Appl. Mater. Interfaces*, 2015, **7**, 3655.
- 281 Z. Chen, W. Ren, L. Gao, B. Liu, S. Pei and H. Cheng, *Nat. Mater.*, 2011, **10**, 424.
- 282 Y. Zhu, S. Murali, M. Stoller, K. Ganesh, W. Cai, P. Ferreira, A. Pirkle, R. Wallace, K. Cychosz, M. Thommes, D. Su, E. A. Stach and R. Ruoff, *Science*, 2011, **332**, 1537.
- 283 T. Brousse, D. Belanger, and J. Long, *J. Electrochem. Soc.*, 2015, **162**, A5185.
- 284 P. Simon, Y. Gogotsi, and B. Dunn, *Science*, 2014, **343**, 1210.
- 285 Q. Zhou, X. Wang, Y. Liu, Y. He, Y. Gao, and J. Liu, *J. Electrochem. Soc.*, 2014, **161**, A1922.

## TOC Graphic



## Biographies



**Bing Li** is now a graduate student under Professor Huan Pang's supervision, Yangzhou University of chemistry and chemical engineering, China. Her research mainly focuses on the field of inorganic semiconductors nanostructures and their applications for supercapacitors.



**Mingbo Zheng** received his Ph.D. in material processing engineering from Nanjing University of Aeronautics and Astronautics in 2009. He was a postdoctoral researcher at Nanjing University from 2009 to 2012. He was an associate researcher at Nanjing University from 2012 to 2015. He is currently an associate professor at Yangzhou University. His research interests are in the field of materials for energy storage, including lithium-ion battery, lithium-sulfur battery, lithium-air battery, and supercapacitor.



**Huaiguo Xue** received his Ph.D. degree in polymer chemistry from the Zhejiang University in 2002. He is currently a professor of physical chemistry and the dean of the

College of Chemistry and Chemical Engineering at the Yangzhou University. His research interests focuses on electrochemistry, functional polymer and biosensors.



**Huan Pang** received his Ph. D. degree from Nanjing University in 2011. He then founded his research group in Anyang Normal University where he was appointed as a distinguished professor in 2013. He has now joined Yangzhou University as a university distinguished professor. His research interests include the development of inorganic semiconductors nanostructures and their applications in flexible electronics with a focus on energy devices.